2014-06

Design and optimization of Copper Indium Gallium Selenide solar cells for lightweight battlefield application

Columbus, Douglas A.

Monterey, California: Naval Postgraduate School

NAVAL POSTGRADUATE SCHOOL

MONTEREY, CALIFORNIA

THESIS

DESIGN AND OPTIMIZATION OF COPPER INDIUM GALLIUM SELENIDE SOLAR CELLS FOR LIGHTWEIGHT BATTLEFIELD APPLICATION

by

Douglas A. Columbus

June 2014

Thesis Advisor: Sherif Michael
Second Reader: Daniel Nussbaum

Approved for public release; distribution is unlimited

THIS PAGE INTENTIONALLY LEFT BLANK

REPORT DOCUMENTATION PAGE

Form Approved OMB No. 0704-0188

1. AGENCY USE ONLY *(Leave blank)*	**2. REPORT DATE** June 2014	**3. REPORT TYPE AND DATES COVERED** Master's Thesis

4. TITLE AND SUBTITLE
DESIGN AND OPTIMIZATION OF COPPER INDIUM GALLIUM SELENIDE SOLAR CELLS FOR LIGHTWEIGHT BATTLEFIELD APPLICATION

5. FUNDING NUMBERS

6. AUTHOR(S) Douglas A. Columbus

7. PERFORMING ORGANIZATION NAME(S) AND ADDRESS(ES)
Naval Postgraduate School
Monterey, CA 93943-5000

8. PERFORMING ORGANIZATION REPORT NUMBER

9. SPONSORING /MONITORING AGENCY NAME(S) AND ADDRESS(ES)
N/A

10. SPONSORING/MONITORING AGENCY REPORT NUMBER

11. SUPPLEMENTARY NOTES The views expressed in this thesis are those of the author and do not reflect the official policy or position of the Department of Defense or the U.S. Government. IRB Protocol number ____N/A____.

12a. DISTRIBUTION / AVAILABILITY STATEMENT
Approved for public release; distribution is unlimited

12b. DISTRIBUTION CODE

13. ABSTRACT (maximum 200 words)

The design and optimization of higher efficiency Copper Indium Gallium Selenide (CIGS) solar cells are investigated in this thesis. Optimizing the thickness layers of a cell for various band gaps was conducted in order to design a cell that exceeds the current industry efficiency record of 20.8%. Silvaco provides a modeling program called ATLAS that is specifically designed to model semiconductor devices. ATLAS was used to model a CIGS cell that is currently being produced to verify the validity of the model. Various thicknesses were then swept to determine the optimum thickness for a given band gap.

Solar spectrum intensity varies by location around the Earth. Optimizing CIGS cells for various band gaps yields higher overall power output when dealing with drastic climate and location variations. Cells for five band gaps ranging from 1.14 eV to 1.69 eV were optimized in this thesis. The highest achieved efficiency was for a band gap of 1.69 eV with an overall theoretical efficiency of 22.4%.

14. SUBJECT TERMS CIGS, efficiency, optimization, thickness, band gap, Silvaco, ATLAS	**15. NUMBER OF PAGES** 103
	16. PRICE CODE

17. SECURITY CLASSIFICATION OF REPORT	**18. SECURITY CLASSIFICATION OF THIS PAGE**	**19. SECURITY CLASSIFICATION OF ABSTRACT**	**20. LIMITATION OF ABSTRACT**
Unclassified	Unclassified	Unclassified	UU

NSN 7540-01-280-5500

Standard Form 298 (Rev. 2-89)
Prescribed by ANSI Std. 239-18

THIS PAGE INTENTIONALLY LEFT BLANK

Approved for public release; distribution is unlimited

DESIGN AND OPTIMIZATION OF COPPER INDIUM GALLIUM SELENIDE SOLAR CELLS FOR LIGHTWEIGHT BATTLEFIELD APPLICATION

Douglas A. Columbus
Captain, United States Marine Corps
B.S. United States Naval Academy, 2008

Submitted in partial fulfillment of the
requirements for the degree of

MASTER OF SCIENCE IN ELECTRICAL ENGINEERING

from the

NAVAL POSTGRADUATE SCHOOL
June 2014

Author: Douglas A. Columbus

Approved by: Dr. Sherif Michael
Thesis Advisor

Dr. Daniel Nussbaum
Second Reader

Dr. R. Clark Robertson
Chair, Department of Electrical and Computer Engineering

THIS PAGE INTENTIONALLY LEFT BLANK

ABSTRACT

The design and optimization of higher efficiency Copper Indium Gallium Selenide (CIGS) solar cells are investigated in this thesis. Optimizing the thickness layers of a cell for various band gaps was conducted in order to design a cell that exceeds the current industry efficiency record of 20.8%. Silvaco provides a modeling program called ATLAS that is specifically designed to model semiconductor devices. ATLAS was used to model a CIGS cell that is currently being produced to verify the validity of the model. Various thicknesses were then swept to determine the optimum thickness for a given band gap.

Solar spectrum intensity varies by location around the Earth. Optimizing CIGS cells for various band gaps yields higher overall power output when dealing with drastic climate and location variations. Cells for five band gaps ranging from 1.14 eV to 1.69 eV were optimized in this thesis. The highest achieved efficiency was for a band gap of 1.69 eV with an overall theoretical efficiency of 22.4%.

THIS PAGE INTENTIONALLY LEFT BLANK

TABLE OF CONTENTS

I. INTRODUCTION....1
A. BACKGROUND....1
B. RELATED RESEARCH AT NPS....2
C. RESEARCH OBJECTIVE....2
D. STRUCTURE OF THESIS....3

II. BATTLEFIELD APPLICATIONS OF SOLAR CELLS....5
A. INTRODUCTION....5
B. GROUND RENEWABLE EXPEDITIONARY ENERGY SYSTEM....5
C. SOLAR PORTABLE ALTERNATIVE COMMUNICATIONS ENERGY SYSTEM....6
D. MARINE AUSTERE PATROLLING SYSTEM....7
E. CIGS PANELS....9

III. THEORETICAL BACKGROUND....13
A. PHYSICS OF SOLAR CELLS....13
1. Photovoltaic Effect in Semiconductors....13
2. Solar Cell Operation....14
a. Doping....14
b. P-N Junction....15
c. Photo Current Generation....17
3. Solar Non-Idealities....17
4. Types of Solar Cells....18
B. SOLAR SPECTRA IRRADIATION ON EARTH....19
C. THIN FILM SOLAR CELL....20
1. Amorphous Si....21
2. CdTe....21

IV. CIGS SOLAR CELLS....23
A. BASIC STRUCTURE....23
1. Substrate....23
2. Back Contact....24
3. Absorber Layer....24
4. Buffer Layer....25
5. Window Layer....25
B. ADJUSTING THE BAND GAP....25
C. BENEFITS OF CIGS CELLS MANUFACTURING....28
1. Inexpensive Manufacturing....28
2. Flexible....30
3. Lightweight....30
D. CURRENT STATE OF TECHNOLOGY.....30
E. CONCLUSION....32

V. SIMULATION AND RESULTS....33

A. SILVACO BASICS 33
B. SOFTWARE CONFIRMATION 34
1. Basic Cell Confirmation 34
2. Band Gap Confirmation 36
C. OPTIMIZATION 39
1. Individual Sweeps 39
2. Combined Sweep 42
D. FINAL RESULTS 45

VI. CONCLUSION 47
A. CONCLUSION 47
B. RECOMMENDATIONS FOR FUTURE WORK 48
1. Physical Confirmation of Model 48
2. Model Improvement 48
3. Currently Manufactured Cell Parameters 48
4. Additional Solar Spectrums 48
5. Higher Efficiency CIGS Concepts 48

APPENDIX A. DEVICE BASIC CONSTRUCTION AND LAYOUT 51
A. STRUCTURE SPECIFICATION 51
1. Mesh 52
2. Region 53
3. Electrode 54
4. Doping 54
B. MATERIALS MODELS SPECIFICATION 54
1. Material 54
2. Models 55
C. NUMERIC METHOD SELECTION 55
D. SOLUTION SPECIFICATION 55
1. Log 56
2. Solve 56
3. Load 56
4. Save 56
E. RESULTS ANALYSIS 57

APPENDIX B. ATLAS SOURCE CODE 59
A. BASELINE CIGS CELL FILE 59
B. CIGS CELL SWEEP FILE 60

APPENDIX C. ADDITIONAL BAND GAP CELL RESULTS 63
A. GALLIUM OF 10% WITH BAND GAP OF 1.14 eV 63
B. GALLIUM OF 50% WITH BAND GAP OF 1.41 eV 66
C. GALLIUM OF 70% WITH BAND GAP OF 1.55 eV 69
D. GALLIUM OF 90% WITH BAND GAP OF 1.69 eV 72

LIST OF REFERENCES 75

INITIAL DISTRIBUTION LIST 79

LIST OF FIGURES

Figure 1. GREENS being utilized by Marines in the field, from [7]. 6
Figure 2. SPACES being utilized by Marines in the field, from [9]. 7
Figure 3. MicroLink Devices, Inc. triple junction solar cell, from [10]. 8
Figure 4. CIGS cell being rolled onto itself. 9
Figure 5. General purpose tent covered with solar cells, from [14]. 10
Figure 6. Solar panels mounted on a standard shipping container, from [14]. 11
Figure 7. Energy Structures of Conductors, Semiconductors, and Insulators, from [15]. 13
Figure 8. Flow of an electron and hole in a semiconductor with an electric field applied. 14
Figure 9. Crystalline Si doped with a phosphorous atom, from [16]. 15
Figure 10. Crystalline Si doped with an aluminum atom, from [16]. 15
Figure 11. A p-n junction at equilibrium, from [18]. 16
Figure 12. Charge creation and separation, from [19]. 17
Figure 13. Photoelectric affect in solar cells, from [15]. 18
Figure 14. Solar spectral irradiance versus wavelength for differing standards, from [15]. 19
Figure 15. Layers of an amorphous Si solar cell, from [21]. 21
Figure 16. Layers of CdTe solar cell, from [24]. 22
Figure 17. CIGS basic structure, from [25]. 23
Figure 18. Quantum efficiency curves for CIGS solar cells with different relative Ga content giving band gaps of (a) 1.02 eV, (b) 1.16 eV, and (c) 1.4 eV, from [29]. 27
Figure 19. Current-voltage curves for CIGS solar cells with different relative Ga content giving band gaps of (a) 1.02 eV, (b) 1.16 eV, and (c) 1.4 eV, from [29]. 28
Figure 20. Roll-to-roll processing of CIGS solar cells, from [33]. 29
Figure 21. NREL's best research-cell efficiencies versus time, from [35]. 31
Figure 22. ATLAS inputs and outputs, from [28]. 33
Figure 23. Control cells used as the basis of simulation. 35
Figure 24. Extrapolated graph of Ga content versus band gap. 37
Figure 25. IV curves of the control cells with varying Ga content. 38
Figure 26. Quantum efficiency versus wavelength for CIGS cells with five different band gaps illuminated with AM0. 39
Figure 27. Sweep of iZnO thickness from 0.05 to 0.1 µm versus cell efficiency. 40
Figure 28. Sweep of CdS thickness from 0.05 to 0.1 µm versus cell efficiency. 41
Figure 29. Sweep of CIGS thickness from 1.0 to 2.5 µm versus cell efficiency. 42
Figure 30. Optimization trial run versus cell efficiency. 44
Figure 31. IV curves of Initial Cell and Optimized Cell. 44
Figure 32. IV curves of the optimized cells with varying Ga content. 46
Figure 33. Categories of statement used in DeckBuild, from [28] 51
Figure 34. Mesh with vertical lines every 0.1 µm from $x = -1$ to $x = 1$. 52

Figure 35. Sweep of iZnO thickness from 0.05 to 0.1 µm versus cell efficiency. 63
Figure 36. Sweep of CdS thickness from 0.05 to 0.1 µm versus cell efficiency. 63
Figure 37. Sweep of CIGS thickness from 1.0 to 2.5 µm versus cell efficiency. 64
Figure 38. Optimization trial run from Table 6 versus cell efficiency. 65
Figure 39. IV curves of initial cell and optimized cell. 65
Figure 40. Sweep of iZnO thickness from 0.05 to 0.1 µm versus cell efficiency. 66
Figure 41. Sweep of CdS thickness from 0.05 to 0.1 µm versus cell efficiency. 66
Figure 42. Sweep of CIGS thickness from 1.0 to 2.5 µm versus cell efficiency. 67
Figure 43. Optimization trial run from Table 7 versus cell efficiency. 68
Figure 44. IV curves of initial cell and optimized cell. 68
Figure 45. Sweep of iZnO thickness from 0.05 to 0.1 µm versus cell efficiency. 69
Figure 46. Sweep of CdS thickness from 0.05 to 0.1 µm versus cell efficiency. 69
Figure 47. Sweep of CIGS thickness from 1.0 to 2.5 µm versus cell efficiency. 70
Figure 48. Optimization trial run from Table 8 versus cell efficiency. 71
Figure 49. IV curves of initial cell and optimized cell. 71
Figure 50. Sweep of iZnO thickness from 0.05 to 0.1 µm versus cell efficiency. 72
Figure 51. Sweep of CdS thickness from 0.05 to 0.1 µm versus cell efficiency. 72
Figure 52. Sweep of CIGS thickness from 1.0 to 2.5 µm versus cell efficiency. 73
Figure 53. Optimization trial run from Table 9 versus cell efficiency. 74
Figure 54. IV curves of initial cell and optimized cell. 74

LIST OF TABLES

Table 1. Semiconductor material parameters.....36
Table 2. Measurements from IV curves in Figure 25. 38
Table 3. Optimization trial run with corresponding thicknesses and efficiency.....43
Table 4. Comparison of control cell efficiency with optimized cell efficiency.....45
Table 5. Measurements from IV curves in Figure 32. 46
Table 6. Optimization trial run with corresponding thicknesses and efficiency.....64
Table 7. Optimization trial run with corresponding thicknesses and efficiency.....67
Table 8. Optimization trial run with corresponding thicknesses and efficiency.....70
Table 9. Optimization trial run with corresponding thicknesses and efficiency.....73

THIS PAGE INTENTIONALLY LEFT BLANK

LIST OF ACRONYMS AND ABBREVIATIONS

CdS	cadmium sulfide
CdTe	cadmium telluride
CGS	copper gallium di-selenide ($CuGaSe_2$)
CIGS	copper indium gallium di-selenide, $Cu(In,Ga)Se_2$
CIS	copper indium di-selenide ($CuInSe_2$)
CMC	Commandant of the Marine Corps
E_g	band gap energy
eV	electron volt
Ga	gallium
Ge	germanium
GREENS	ground renewable expeditionary energy system
HEPV	high efficiency photovoltaic
I_{SC}	short circuit current
IV	current vs. voltage
iZnO	intrinsic zinc oxide
MAPS	Marine austere patrolling system
Mo	molybdenum
NPS	Naval Postgraduate School
Si	silicon
SLG	soda lime glass
SPACES	solar portable alternative communications energy system
TCO	transparent conducting oxide
V_{OC}	open circuit voltage
ZnO	zinc oxide

THIS PAGE INTENTIONALLY LEFT BLANK

EXECUTIVE SUMMARY

As energy demand continues to rise, the need for renewable energy sources is increasingly evident. This need is even greater for expeditionary military forces which cannot rely on grid power for many of their systems. While technology and innovation continues to improve the lethality of military forces, it also presents an ever increasing energy demand. Logistical resupply has responded with more convoys supplying units with fuel for generators and non-rechargeable batteries. In the presence of improvised explosive devices and ambushes, these convoys represent unnecessary risk to friendly forces and supply lines. This presents a clear need for renewable energy sources.

Solar cells, at present, are one of the most widespread forms of renewable energy in the civilian and military domains. Several solar projects have been commissioned by the Marine Corps for stationary units, mobile units, and patrolling Marines [1]–[3]. As technology advances, these systems have become smaller and more efficient. However, cost has not been shown to decrease proportional to technological advancement. In the face of decreasing budgets and cuts to military spending, the need for efficient and inexpensive solar cells is desired.

Thin film solar cells present an attractive option due to their light weight and flexible nature. Leading the thin film market are cells constructed from copper indium gallium di-selenide (CIGS), a compound quaternary semiconductor alloy. The robust material properties of CIGS cells present many attractive features for both military and consumer applications, such as mechanical flexibility and durability. One of the most desirable traits is low cost of CIGS cell manufacture. Although CIGS cells currently lack the efficiency of silicon-based cells or more advanced multi-junction cells, continued research shows promise in closing this gap while still retaining all the desired qualities of CIGS. Optimization of the design parameters of CIGS structures is necessary to fully maximize the capabilities of cells which will be used in future systems.

The objective of this research is to optimize the thickness of the semiconductor layers in CIGS cells for five band gaps. The goal is to increase solar cell efficiency for

CIGS cells designed for a specified location or climate. The sun produces light at varying intensities throughout the wavelength spectrum. As light passes through the Earth's atmosphere, it is absorbed and reflected, resulting in reduced light intensity. This reduction is not uniform throughout the Earth. Regions close to the equator receive more intense and direct sun light, while the polar regions receive weaker, glancing rays. Manipulating the band gap of CIGS by varying the mole fraction of gallium allows us to target the most ideal wavelengths of light for a given region. The Marine Corps' primary purpose is to be an expeditionary force in readiness. This requires Marines to deploy at a moment's notice to austere environments where electrical power is at a premium. Having cells specifically designed for the climate or region of operations will result in higher power output and extend operational endurance.

A CIGS cell is modeled in this thesis using the program called ATLAS provided by Silvaco. An initial cell was created based on published designs from [4]–[6] to validate the model. Cells with band gaps of 1.14 eV, 1.27 eV, 1.41 eV, 1.55 eV, and 1.69 eV were created, and the baseline performance for each cell was recorded. The modeled CIGS cells contained three layers of semiconductor material; intrinsic zinc oxide (iZnO), cadmium sulfide (CdS), and CIGS. The basic cell design is displayed in Figure 1.

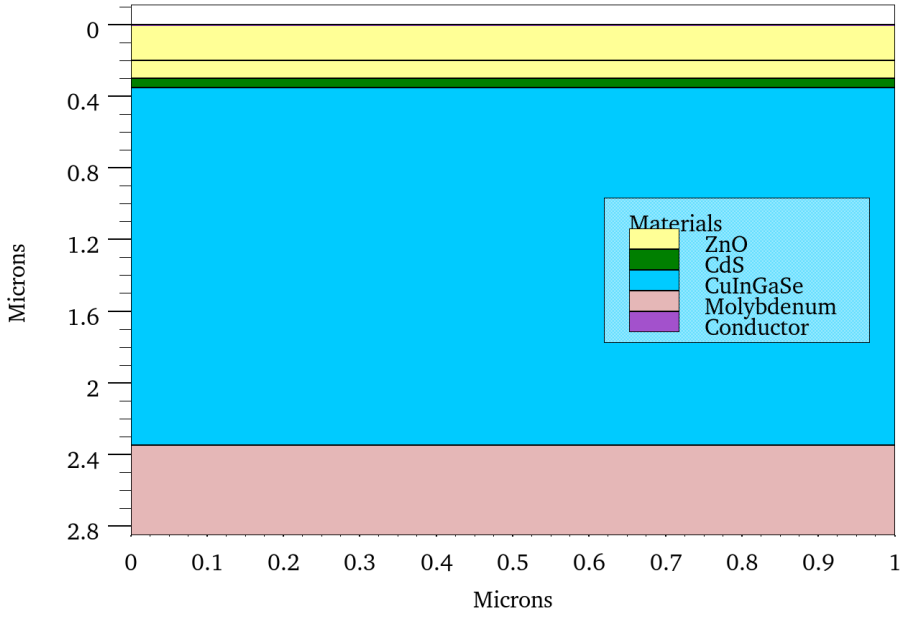

Figure 1. Basic cell structure used.

Individual sweeps were first conducted by holding all variables constant and only varying the thickness of a single semiconductor layer. This method allowed for the examination of how a CIGS cell reacts to variations of a single parameter. The individual sweeps showed trends that were observed in every band gap cell tested. Cell efficiency decreased as iZnO increased; however, the efficiency proved to be very insensitive to the iZnO thickness. This is due to the fact that iZnO is used to aid in the manufacturing process and does not directly impact carrier generation. The optimum iZnO thickness was determined to be 0.05 μm. CdS showed a slight efficiency increase before an exponential drop. Increasing CdS beyond 0.06 μm thickness shadows the CIGS layer thereby reducing efficiency. The CIGS layer showed a continual increase in efficiency as thickness was increased. This can be contributed to more carriers being generated and a higher short circuit current. CIGS thickness exhibited a law of diminishing returns where increasing the thickness resulted in smaller and smaller efficiency gains. CIGS thickness was limited to 2.5 μm in order to retain the thin and flexible properties of the cell.

A combined sweep was then required in order to evaluate how changing each layer affects the performance of the cell with regard to the others. To conduct the combined sweep, thicknesses from each of the individual sweeps needed to be chosen. The two thicknesses from each semiconductor layer that yielded the highest efficiencies were kept and swept against each other. This resulted in a combined sweep of eight trial runs to determine the semiconductor thicknesses that achieved maximum efficiency.

The process of individual sweeps followed by a combined sweep was then repeated four times for the remaining band gap cells. Through this process, the five band gap cells all achieved higher efficiencies. A comparison of the control cell efficiency, the optimized cell efficiency, and the percent improvement achieved is displayed in Table 1.

Table 1. Comparison of control cell efficiency with optimized cell efficiency.

Ga content	0.1	0.3	0.5	0.7	0.9
Band Gap (eV)	1.14	1.27	1.41	1.55	1.69
Control Cell	14.25%	17.13%	18.63%	20.04%	21.90%
Optimized Cell	14.31%	17.28%	18.89%	20.40%	22.40%
% Increase	0.421%	0.876%	1.396%	1.796%	2.283%

This simulation succeeded in increasing the efficiency of each cell with the highest band gap cell showing the most improvement and a total efficiency of 22.4%. Due to a limitation in ATLAS, only the solar spectrums of AM1.5 or AM0 could be used for this simulation. Nevertheless, the simulation did confirm that CIGS cells of varying band gaps responded differently to the spectrum of AM1.5.

Recommendations for future work include:

1. Physical Confirmation of Model

Confirming the model is an important step in this research; however, it is not a sufficient substitute to physical confirmation. CIGS cells with varying band gaps need to be produced and tested in contrasting geographic locations or solar irradiance to confirm the concept presented in this thesis.

2. Model Improvement

Additional research is required in order to improve the ATLAS model used in this thesis. Research into how manufacturing defects affect the performance and how to model these characteristics will produce a more accurate model. Electron hole mobility and lifetime also need to be more accurately modeled for higher band gap CIGS material.

3. Currently Manufactured Cell Parameters

Parameters for CIGS cells that are currently being manufactured need to be attained and added to the model. The lack of these parameters is due to company's reluctance to freely publish designs that required thousands of dollars and man hours to determine. By obtaining real world parameters, a more accurate model can be created and confirmed.

4. Additional Solar Spectrums

Designing solar cells that were specifically tuned to the solar irradiance of a region was the goal of this thesis. In order to fully validate this concept, additional solar irradiance profiles need to be entered into ATLAS. Currently Silvaco and ATLAS contain the standard spectrums of AM0 and AM1.5. By entering measured solar irradiance into the model, a true optimum band gap cell can be developed and tested.

5. Higher Efficiency CIGS concepts

With CIGS ability to vary band gap, differing designs can be tested in an attempt to achieve higher efficiency cells. A dual junction CIGS cell can be attempted by placing a higher band gap CIGS material above a lower band gap one. Another concept is to design a CIGS layer that continually changes band gap with thickness. The top of the CIGS layer would be high band gap material and then gradually transition to lower band gaps towards the bottom of the cell. This gradient could present the benefits of a multi-junction cell without the need for tunnel junctions between layers of different materials.

LIST OF REFERENCES

[1] Office of Naval Research. Ground Renewable Expeditionary Energy System [Online]. Available: http://www.onr.navy.mil/Media-Center/Fact-Sheets/Greens-Solar-Energy-Battery.aspx

[2] A. R. Harvey, "The modification of HOMER software application to provide the United States Marine Corps with an energy planning tool," M.S. thesis, Dept. Elec. Eng., Naval Postgraduate School, Monterey, CA, 2012.

[3] Triple-Junction ELO Tabbed Solar Cell for Portable Power Applications, MicroLink Devices, Inc., Niles, IL, 2012.

[4] M. Hsieh, S. Kuo, F. Lai, M. Kao, P. Huang, H. W. Wang, M. Tsai, and H. Kuo, "Optimization of CdS buffer layer on the performance of copper indium gallium selenide solar cells," in *Proceedings of the International Quantum Electronics Conf. and Conf. on Lasers and Electro-Optics Pacific Rim,* Sydney, Australia, 2011, pp. 1532–1534.

[5] A. H. Jahagirdar, A. A. Kadam, N. and G. Dhere, "Role of i-ZnO in optimizing open circuit voltage of CIGS2 and CIGS thin film solar cells," in *Conf. Record of the IEEE 4th World Conf., Photovoltaic Energy Conversion,* Waikoloa, HI, 2006, pp. 557–559.

[6] T. Nakada, T. Kuraishi, T. Inoue, and T. Mise, "CIGS thin film solar cells on polymide foils," in *Photovoltaic Specialists Conf.*, Honolulu, HI, 2010, pp. 330-334.

THIS PAGE INTENTIONALLY LEFT BLANK

ACKNOWLEDGMENTS

I would like to first thank my thesis advisor, Dr. Sherif Michael. His guidance and experience was instrumental to the completion of this thesis. I would also like to sincerely thank Research Associate Matthew Porter. He spent numerous hours guiding me through the inner workings of Silvaco ATLAS. His help and guidance throughout this process is what allowed me complete my thesis. Thank you.

I would like to thank my family members for their constant support through all of my trials and tribulations. Their support is what gives me the strength to continue. Thank you for instilling in me a thirst for knowledge and to never quit.

Lastly, I would like to thank my fiancée, Carlee. Her support through my graduate education has been unending. I look forward to graduation and beginning the next chapter of our lives together.

THIS PAGE INTENTIONALLY LEFT BLANK

I. INTRODUCTION

A. BACKGROUND

As energy demand continues to rise, the need for renewable energy sources is increasingly evident. This need is even greater for expeditionary military forces which cannot rely on grid power for many of their systems. While technology and innovation continues to improve the lethality of military forces, it also presents an ever-increasing energy demand. Logistical resupply has responded with more convoys supplying units with fuel for generators and non-rechargeable batteries. In the presence of improvised explosive devices and ambushes, these convoys represent unnecessary risk to friendly forces and supply lines. This presents a clear need for renewable energy sources.

Solar cells, at present, are one of the most widespread forms of renewable energy in the civilian and military domains. Several solar projects have been commissioned by the Marine Corps for stationary units, mobile units, and patrolling Marines. As technology advances, these systems have become smaller and more efficient. However, cost has not been shown to decrease proportional to technological advancement. In the face of decreasing budgets and cuts to military spending, the need for efficient and inexpensive solar cells is desired.

Thin film solar cells present an attractive option due to their light weight and flexible nature. Leading the thin film market are cells constructed from copper indium gallium di-selenide (CIGS), a compound quaternary semiconductor alloy. The robust material properties of CIGS cells present many attractive features for both military and consumer applications, such as mechanical flexibility and durability. One of the most desirable traits is the low cost of manufacturing CIGS cells. Although CIGS cells currently lack the efficiency of silicon (Si) based cells or more advanced multi-junction cells, continued research shows promise in closing this gap while still retaining all the desired qualities of CIGS. Optimization of the design parameters of CIGS structures is necessary to fully maximize the capabilities of cells which will be used in future systems.

B. RELATED RESEARCH AT NPS

Many approaches have been attempted to increase the efficiency of CIGS cells. Consistent with all solar cells, CIGS performance parameters are highly influenced by the thickness, doping and the band gap engineering of each section of the cells, which are grown epitaxially upon a substrate. The work in this thesis relies on previous work at the Naval Postgraduate School (NPS) to build a base parameter cell.

In 2012, LT Konstantinos Fotis of the Hellenic Navy developed a CIGS cell in ATLAS. By varying the mole fraction of gallium (Ga) in CIGS, he created cells with different band gaps. Placing a higher band gap CIGS layer on top of a lower band gap one, he created a rudimentary dual junction cell resulting in a higher efficiency [1]. This approach has not been attempted by industry and was, therefore, not investigated in this thesis.

C. RESEARCH OBJECTIVE

The objective of this research is to optimize the thickness of the semiconductor layers in CIGS cells for five band gaps. The goal is to increase solar cell efficiency for CIGS cells designed for a specified location or climate. The sun produces light at varying intensities throughout the wavelength spectrum. As this light passes through the Earth's atmosphere it is absorbed and reflected, resulting in reduced light intensity. This reduction is not uniform throughout the Earth. Regions close to the equator receive more intense and direct sun light, while the polar regions receive weaker glancing rays. Changing the band gaps of CIGS allows us to target the most ideal wavelengths of light for a given region. The Marine Corps primary purpose is to be an expeditionary force in readiness. This requires Marines to deploy at a moment's notice to austere environments where electrical power is at a premium. Having cells specifically designed for the climate or region of operations can result in higher power output and extend operational endurance.

In this thesis, a CIGS cell is modeled using the program called ATLAS provided by Silvaco. An initial cell was created based on published designs from [2]–[4]. Cells with five different band gaps were then created and the baseline performance for each

cell was recorded. The modeled CIGS cells contained three layers of semiconductor material; intrinsic zinc oxide (iZnO), cadmium sulfide (CdS), and CIGS. Each layer thickness was individually varied to determine performance trends and optimum thickness. This process was repeated five times for the five different band gap cells. The cell performance, measured by the power conversion efficiency of the cell, was compared to the published values to verify the validity of the model.

D. STRUCTURE OF THESIS

This thesis is arranged into six chapters. Battlefield application of solar cells is covered in Chapter II. The theoretical background into the physics of solar cells and the solar spectrum is given in Chapter III. An in depth analysis of CIGS cells is given in Chapter IV. An introduction to Silvaco ATLAS and the results of simulation is given in Chapter V. The conclusion with recommendations for future work is given in Chapter VI.

THIS PAGE INTENTIONALLY LEFT BLANK

II. BATTLEFIELD APPLICATIONS OF SOLAR CELLS

A. INTRODUCTION

The year 2009 marked a decisive shift in the way the United States Marine Corps views energy on the battlefield. On August 13, 2009, the Commandant of the Marine Corps (CMC) General James Conway held the first Marine Corps Energy Summit. The focus of this summit was to address the growing energy needs on the battlefield. The summit posed the question of how the Marine Corps as a whole could reduce the need for fossil fuels or grid power while still remaining expeditionary. Following the path laid by his predecessor, the current CMC, General James Amos, released the "United States Marine Corps Expeditionary Energy Strategy and Implementation Plan" in February 2011. In this document General Amos states,

> As a Corps, we have become more lethal, yet we have also become increasingly dependent on fossil fuel. Our growing demand for liquid logistics comes at a price. By tethering our operations to vulnerable supply lines, it degrades our expeditionary capabilities and ultimately put Marines at risk. To maintain our lethal edge, we must change the way we use energy.
>
> The current and future operating environment requires an expeditionary mindset geared toward increased efficiency and reduced consumption, which will make our forces lighter and faster. We will aggressively pursue innovative solutions to reduce energy demand in our platforms and systems, increase our self-sufficiency in our sustainment, and reduce our expeditionary foot print on the battlefield. Transforming the way we use energy is essential to rebalance our Corps and prepare it for the future. [5]

In response to this growing energy need, the Marine Corps has fielded three systems that rely on solar cells to help provide power to Marines in austere environments. Each system is briefly covered, and recommendations for the use of CIGS cells in battlefield applications are given in this chapter.

B. GROUND RENEWABLE EXPEDITIONARY ENERGY SYSTEM

The ground renewable expeditionary energy network system (GREENS) is a large system designed to power a command post. The eight solar cells are rated to produce up

to 1,600 W combined which then charge four, 80 pound batteries. The system as a whole is designed to provide Marines with 300 W of continuous power [6]. A picture of GREENS being utilized is shown in Figure 1.

Figure 1. GREENS being utilized by Marines in the field, from [7].

One of the main drawbacks of GREENS is that it is not particularly portable. The solar cells used in GREENS have a top layer of glass which increases the weight and makes the array brittle. This requires them to be transported in larger and heavier metal cases as seen in Figure 1. The size and weight of this system means that it is not man portable. Two complete GREENS can fit into a standard Marine Corps shipping container [8].

C. SOLAR PORTABLE ALTERNATIVE COMMUNICATIONS ENERGY SYSTEM

The solar portable alternative communications energy system (SPACES) was the next solar program and focused on making a solar power system that was more light weight. The system contained a foldable solar panel, a battery, and a power converter.

The benefit of SPACES is that the system is significantly more light weight and portable. The relative size and footprint of SPACES is displayed in Figure 2.

Figure 2. SPACES being utilized by Marines in the field, from [9].

One of the main drawbacks of SPACES was the extremely low efficiency cells that were being used with the system. In previous thesis work at NPS, the efficiency of the SPACES solar array was measured; it was revealed that SPACES had a maximum efficiency of 7.8% in Monterey, CA, and a calculated efficiency of 8.8% under the best solar conditions [8].

D. MARINE AUSTERE PATROLLING SYSTEM

The Marine austere patrolling system (MAPS) is a new system that combines solar cells with a battery pack as well as water purification. While MAPS has several unique features such as power management and distribution system, the focus of this thesis is solely on the solar array being used. The MAPS uses triple junction, high

efficiency photovoltaic (HEPV) solar cells provided by MicroLink Devices. The individual cells are capable of 31.1% efficiency with an average panel efficiency of 25% [10], [11]. These cells have undergone a process called epitaxial lift-off that allows the cells to be manufactured much thinner than traditional triple junction cells. MicroLink Devices advertises a thickness of less than 40 μm [10]. Manufacturing the cells using epitaxial lift-off does allow the cell to be lighter weight and somewhat flexible; however, due to the crystalline structure of the semiconductor layers used, the cells will never be truly flexible. The process of epitaxial lift-off also increases manufacturing cost. The flexibility of the MicroLink cell before it is encased in a panel is shown in Figure 3.

Figure 3. MicroLink Devices, Inc. triple junction solar cell, from [10].

From Figure 3, it can be seen that the cell flexibility is consistent with a credit card or piece of plastic. This means that when bent beyond a critical point, the crystalline layers of the cell begin to fracture and degrade the performance of the cell. The solution to this has been to design ruggedized housing that prevents the cells from flexing to the point of damage [11].

While flexibility in solar cells designed for combat is a desirable attribute, the main drawback of MAPS is the cost of these solar cells. These HEPV thin solar panels are expensive to manufacture, with initial panels costing upwards of $10,000 by using cells costing $300/W [11], [12]. This cost can mainly be attributed to non-recurring

engineering costs and product development. A target price point of $50/W is the desired end-state for production grade HEPV cells used with MAPS [11], [12].

E. CIGS PANELS

CIGS cells have numerous benefits over traditional solar cells to include being truly flexible, light weight and inexpensive. The control cell used in this thesis was 2.75 μm thick. In addition to being over 1/14th the thickness of the triple junction cell used in MAPS, the chalcopyrite structure of CIGS allows the cell to bend to extreme angles. A CIGS cell that has been rolled so that the ends of the cell are overlapping is depicted in Figure 4.

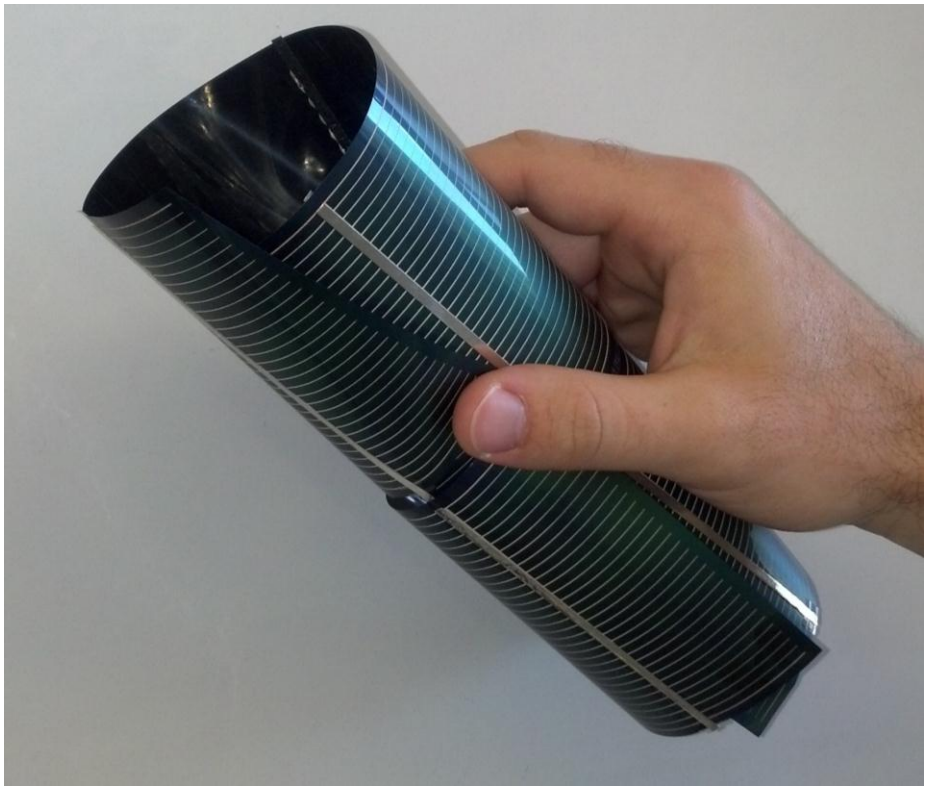

Figure 4. CIGS cell being rolled onto itself.

This property gives a CIGS cell the consistency of a sheet of paper. A sheet of paper can be rolled and twisted without any permanent damage; however, if a crease is made paper does not return to its original form. The same is true for CIGS cells. They can

be rolled and flexed to extreme angles, but if a crease is made, the cell is damaged and efficiency is degraded. The properties that allow CIGS to be manufactured extremely thin also make them lightweight.

The practicality of CIGS is not a result of their unique features but from their affordability. Current CIGS cells are being manufactured for approximately $1/W [13]. In the face of decreasing budgets and a push to acquire commercial-off-the-shelf items, CIGS cells offer a decent efficiency at a bargain price. Additional research has shown the potential for CIGS price to drop to as low as $0.34/W with improved manufacturing techniques and economies of scale [13].

The application of CIGS solar panels for Marine Corps application is explored in this thesis. The lightweight and inexpensive nature of CIGS aligns with the CMC's goal of making our forces lighter and faster. CIGS cells can be made into a small blanket for patrolling Marines or fitted onto larger structures such as General Purpose tents or storage units. The truly flexible nature of CIGS allows the solar panels to be rolled up with a tent, thereby reducing any additional steps or concern. The lower efficiency of CIGS results in a lower power rating per panel; however, the cost savings allows more panels to be purchased. This efficiency cost trade off favors CIGS cells. On average a CIGS panel is 10% less efficient than current triple-junction panels but 1/300th the cost [12], [13]. Potential applications of CIGS in a battlefield environment are shown in Figure 5 and Figure 6.

Figure 5. General purpose tent covered with solar cells, from [14].

Figure 6. Solar panels mounted on a standard shipping container, from [14].

Due to the expeditionary nature of the Marine Corps, a clear need exists for a renewable energy system that can feed the energy demand of modern warfare. This system must be robust enough to withstand the rigors of combat while also being able to withstand the potential for decreasing budgets.

THIS PAGE INTENTIONALLY LEFT BLANK

III. THEORETICAL BACKGROUND

A. PHYSICS OF SOLAR CELLS

1. Photovoltaic Effect in Semiconductors

Solar cells are composed of materials known as semiconductors. Semiconductors are materials that have a band gap in their electronic energy structure. A band gap is the amount of energy that is imparted to an electron to free it from the valence band and move to the conduction band. When this electron is moved to the conduction band it leaves behind a positively charged vacancy known as a hole. The energy structures for conductors, semiconductors, and insulators are displayed in Figure 7.

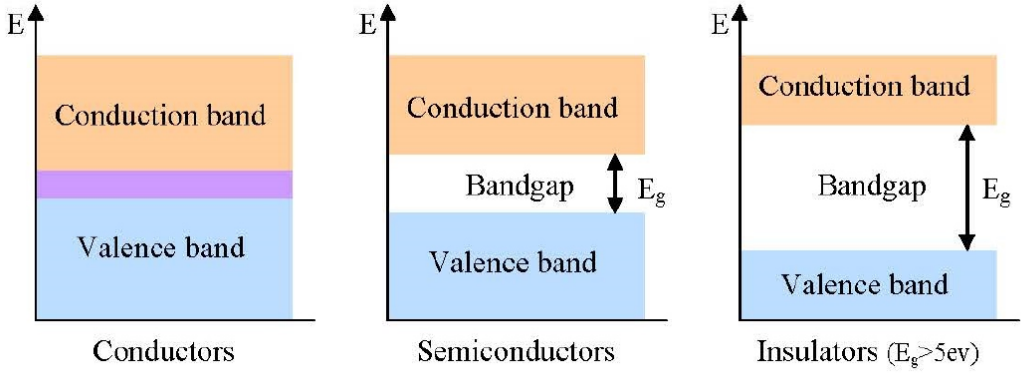

Figure 7. Energy Structures of Conductors, Semiconductors, and Insulators, from [15].

One way electrons can gain energy to overcome the band gap is by absorbing energy *hv* from photons. When an electric field is applied across a semiconductor which has carriers generated due to exposure to light, a net current and positive outflow of energy can be generated. This phenomenon is called photovoltaic effect. The flow of an electron and hole in a semiconductor with an electric field applied is illustrated in Figure 8.

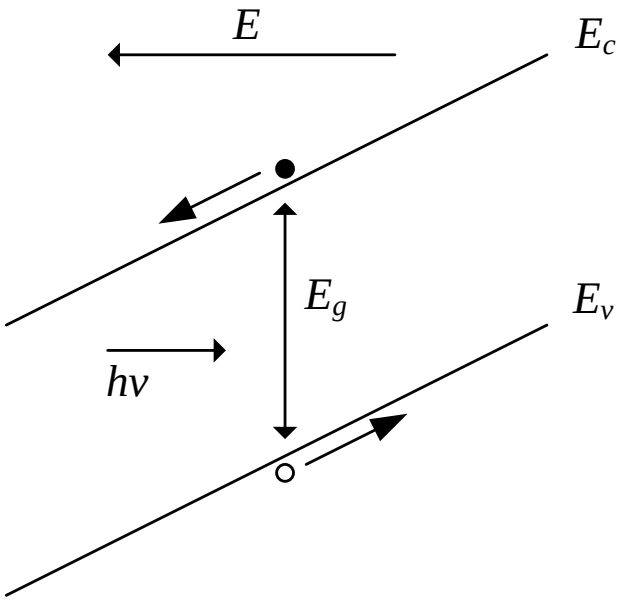

Figure 8. Flow of an electron and hole in a semiconductor with an electric field applied.

Only photons with energy higher than that of the band gap can excite an electron into the conduction band; therefore, each band gap has a maximum wavelength that can free an electron.

2. Solar Cell Operation

a. Doping

The first step in creating a solar cell is to dope the semiconductor. Doping refers to the process of introducing foreign atoms into the structure to alter the properties of the material.

Semiconductors doped with donor elements are considered n-type with electrons being the majority carrier and holes being the minority carrier. A visual representation of crystalline Si doped with phosphorous is depicted in Figure 9.

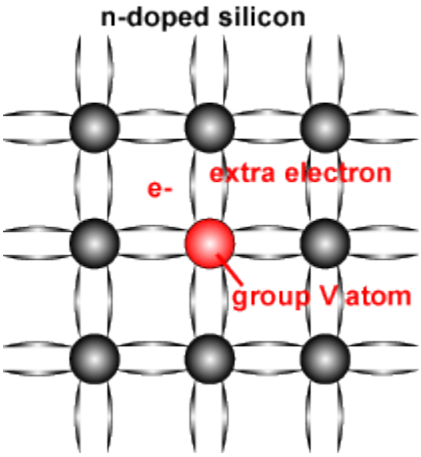

Figure 9. Crystalline Si doped with a phosphorous atom, from [16].

Semiconductors can also be doped with acceptor atoms to create the opposite effect. Acceptor atoms need to accept an electron to bond with a semiconductor. This type of doping is called p-type, where holes represent the majority carriers and electrons are the minority carriers [16]. A sample of Si doped with aluminum is represented in Figure 10.

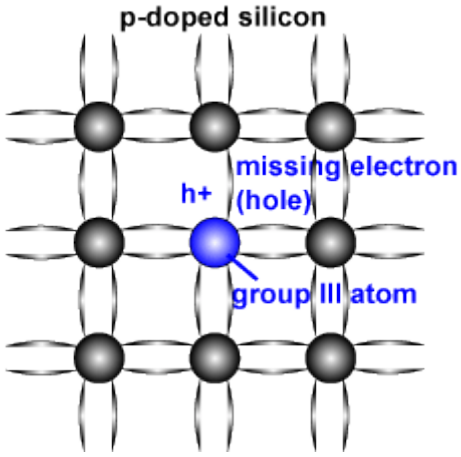

Figure 10. Crystalline Si doped with an aluminum atom, from [16].

b. P-N Junction

P-n junctions are how an internal electric field is created in a semiconductor. A p-n junction is formed by joining a p-type semiconductor with an n-type semiconductor. As

stated before, p-type semiconductors have holes as the majority carriers while n-type semiconductors have electrons. When the two materials are joined, the majority carriers diffuse into the opposite material. From the n-type side, electrons diffuse into the p-type material and combine with the dopant atoms there to create a negative ion. From the p-type side, holes diffuse into the n-type to create positive ions. These ions are bound in the material via the crystalline lattice structure and are, therefore, immobile. This region of positive and negative ions is known as the depletion region. The buildup of positive and negative ions on opposite sides of the boundary forms an electric field. This electric field opposes the diffusion of the majority carriers but remains small at first. As majority carriers cross the boundary and create more charged ions, the electric field grows in strength. This process continues until equilibrium is reached. Equilibrium is achieved when the diffusion force is equal and opposite of the electric field force [17]. The outcome of joining a p-n junction is depicted in Figure 11.

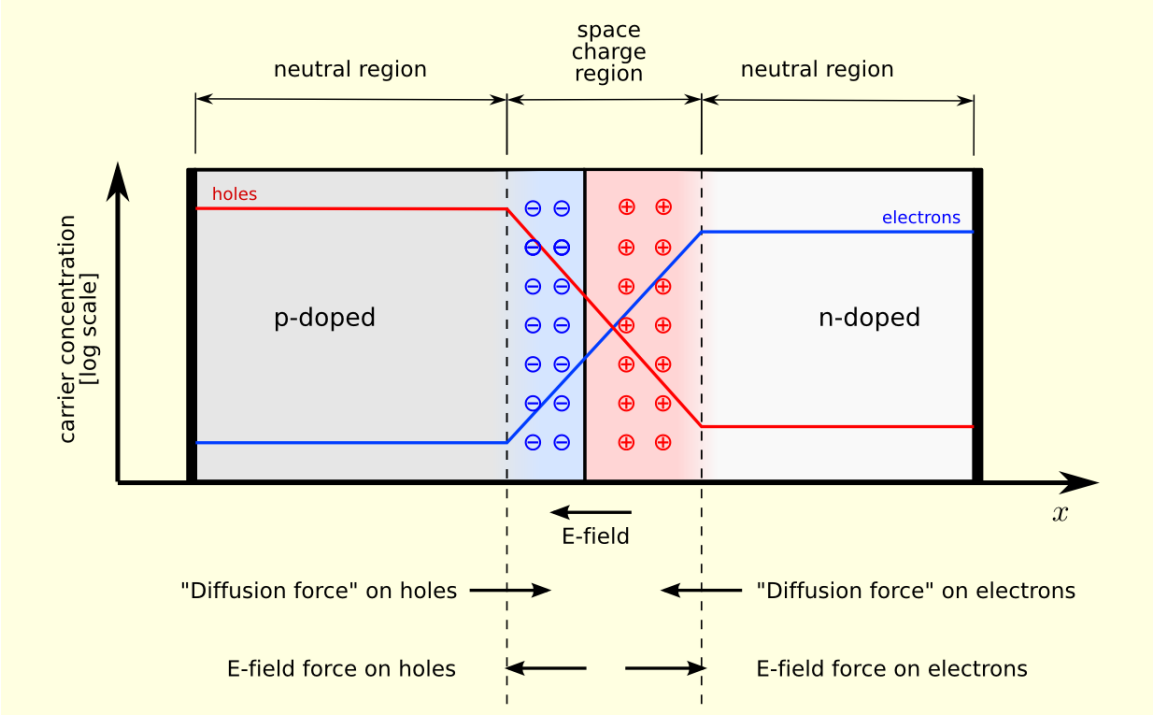

Figure 11. A p-n junction at equilibrium, from [18].

This electric field is crucial for the operation of solar cells. The strength of the electric field is controlled by the concentration dopants in both p and n regions. While the electric field opposes the diffusion of majority carriers, it helps to sweep the minority carriers through the depletion region.

c. Photo Current Generation

When the solar cell is illuminated, some of the photons will have energy above the band gap of the semiconductor material. When a high energy photon strikes an electron, it frees the electron from its bond creating an electron hole pair. This pair is separated by the electric field created by the depletion region. Charge creation and separation is shown in Figure 12.

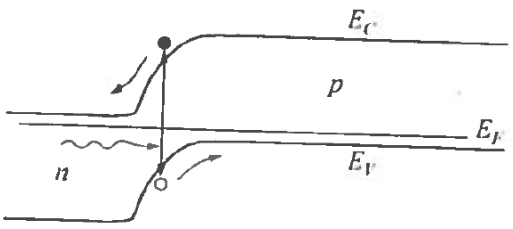

Figure 12. Charge creation and separation, from [19].

The result of illuminating the solar cell is a buildup of excess electrons in the n-region and holes in the p-region. By connecting the terminals of the cell to a load, excess electrons and holes flow through the load to recombine and counteract each other. The maximum current that a solar cell can produce occurs when the terminals are shorted together. This maximum current is called short circuit current, I_{SC}. Applying a load with a resistance creates a voltage in the cell and forward biases the p-n junction. This forward bias reduces the amount of current that the cell can provide to the load. The point at which no current flows with called the open circuit voltage, V_{OC} [1].

3. Solar Non-Idealities

There are several factors that can degrade the performance of solar cells. Primary losses can include reflection of photons off the surface of the cell, shading from the top

grid, photons that are below band gap, and recombination losses. Typical losses in solar cells are depicted in Figure 13.

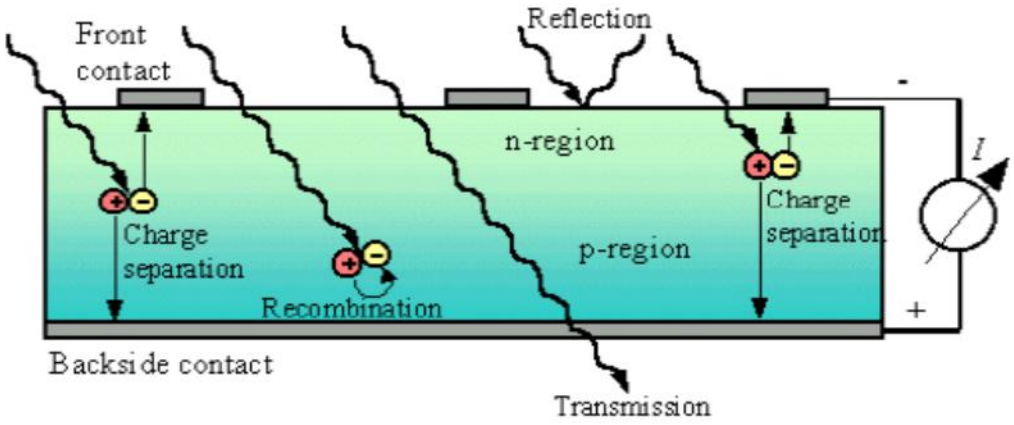

Figure 13. Photoelectric affect in solar cells, from [15].

An in-depth explanation of solar cell losses is found in [20]. Optimizing solar cell efficiencies by targeting the correct band gap and optimum cell thickness for absorption is investigated in this thesis.

4. Types of Solar Cells

There are three broad categories of solar cells. The first is single crystalline Si or crystalline germanium (Ge). These cells were some of the first solar cells produced and still hold a large portion of the market share.

The second types of solar cells are multi-junction cells. These cells stack higher band gap semiconductor material on top of lower band gaps. This process more effectively utilizes the solar spectrum resulting in higher efficiencies. One drawback of multi-junction cells is the increased cost associated with more complex manufacturing process.

The third types of solar cells are thin film cells. These cells utilize direct band gap semiconductors with a high absorption rate. These attributes allow the cells to be manufactured with thin semiconductor layers when compared to the other type of solar cells. Thin film solar cells are discussed in depth in section C of this chapter.

B. SOLAR SPECTRA IRRADIATION ON EARTH

The sun produces light at various intensities throughout the wavelength spectrum. These intensities are closely mimicked by a 6000 K black body radiation. As the light travels through space, its intensity decreases by a rate of $1/d^2$ where d is the distance from the sun [16]. The standard for measuring light intensity on earth is to describe by how many atmospheres the light has passed through. The intensity spectrum for satellites in space is labeled as AM0, since the light has not passed through any of the earth's atmosphere. At sea level, near the equator, at noon on a cloudless day, the spectrum is labeled as AM1, since light has passed through one standard atmosphere. As not all solar cells are utilized on the equator at noon, the industry standard for measuring solar cell is AM1.5, or one and a half atmospheres. Intensity losses in this spectrum are due to photon absorption by particulates in the atmosphere. The most notable of these are ozone (O_3), water (H_2O), and carbon dioxide (CO_2) [16]. These absorption losses are represented by deep troughs as seen in Figure 14.

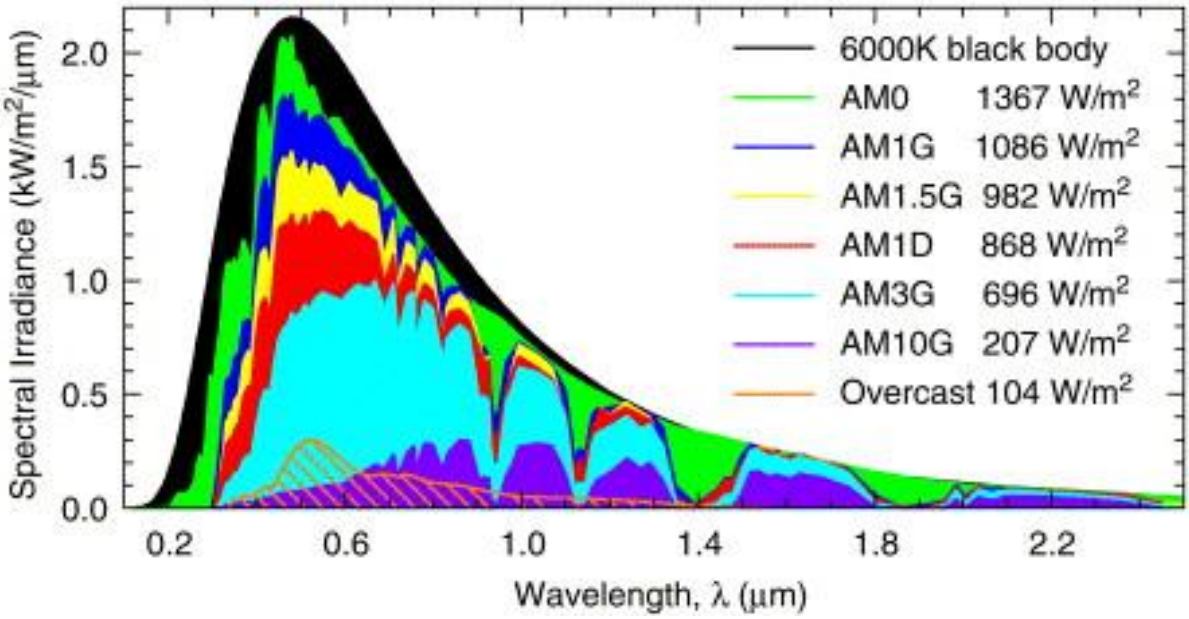

Figure 14. Solar spectral irradiance versus wavelength for differing standards, from [15].

While absorption losses are represented as deep troughs in the spectrum, this does not account for the general loss of intensity. General intensity loss is due to reflection and scattering of photons by air molecules and dust particles in the atmosphere [16].

As stated earlier, the industry standard is AM1.5. This spectrum gives a relative baseline for which all solar cells are tested against. AM1.5 is not representative of the solar spectrum at all locations on the Earth; it is merely used for standardization. Besides atmospheric effects, spectrum intensity is most influenced by altitude, humidity, and latitude. Solar cells at higher altitudes are exposed to more intense radiation than those at sea level. An arid climate has less photon absorption by water molecules than a humid climate. Solar cells used near the equator have more direct sunlight than a cell used at higher latitudes with glancing rays. All of these effects can vary the solar spectrum intensity and change the performance of solar cells. By tuning the band gap of CIGS, we can optimize cells for a particular region or climate. A cell that is used in a high altitude desert might have a different optimum band gap than one used at sea level in 100% humidity. By using a cell with an optimized band gap, average power output can be increased without significant changes in the manufacturing process.

C. THIN FILM SOLAR CELL

Traditional solar cells based on Si and Ge formed the basis of all solar cells today. The early solar cell market was dominated by space applications, where power efficiency is given top design priority with price and large scale manufacturing being relatively neglected. This led companies to produce multi-junction solar cells that achieved record efficiencies at high cost. While solar cells of this caliber are within the grasp of government backed space programs, the average consumer can obviously not afford this solution.

Due to this gap in the market, initiatives to produce cheap, reliable and efficient solar cells for consumer application have been widely researched over the last few decades. Various materials have been investigated to improve solar cell manufacture. There are three main types of solar cells that are leading the thin film market. They are

amorphous Si, cadmium telluride (CdTe), and CIGS. Amorphous Si and CdTe are discussed briefly in this section while CIGS cells are discussed in depth in Chapter IV.

1. Amorphous Si

Amorphous Si is a material used in thin film solar cells for its high absorption rate. Unlike crystalline Si, amorphous Si does not have a uniform crystal structure. It is rather a conglomeration of smaller crystals that are deposited onto a material. By avoiding the costly process of growing a single continuous crystalline Si structure, amorphous Si significantly reduces the manufacturing cost. "Amorphous silicon absorbs solar radiation 40 times more efficiently than does single-crystal silicon, so a film only about 1 micrometer…thick can absorb 90% of the usable light energy shining on it." [21] A typical configuration of an amorphous Si solar cell is shown in Figure 15. More detail on higher efficiency amorphous Si cells can be found in [22].

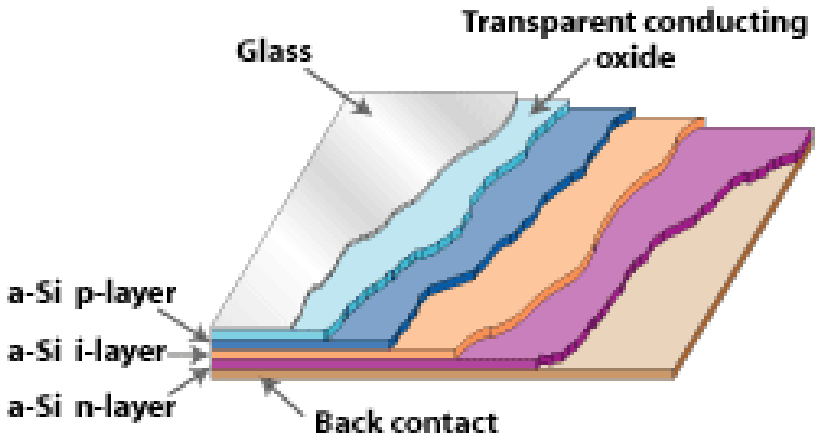

Figure 15. Layers of an amorphous Si solar cell, from [21].

2. CdTe

A second thin film solar cell material on the market is CdTe. CdTe is a combination of a group II and group VI elements to form a crystalline structure. Like amorphous Si, CdTe possesses an extremely high absorption rate allowing it to be manufactured in very thin layers. A typical structure of CdTe is depicted in Figure 16. More detailed information on high efficiency CdTe solar cells can be found in [23].

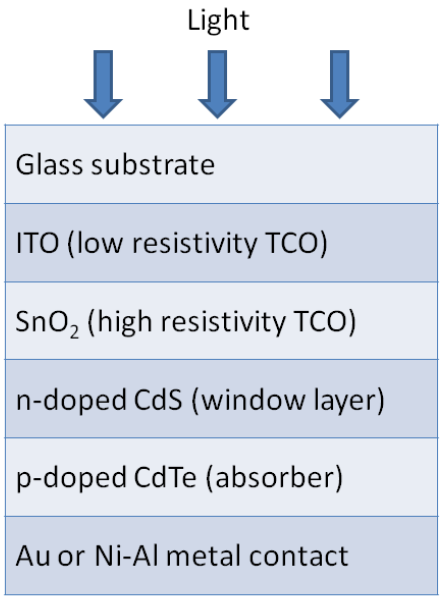

Figure 16. Layers of CdTe solar cell, from [24].

IV. CIGS SOLAR CELLS

A. BASIC STRUCTURE

Modern commercially produced CIGS cells consist of five layers, each with their own unique parameters and function. The typical design of a CIGS cell is shown in Figure 17.

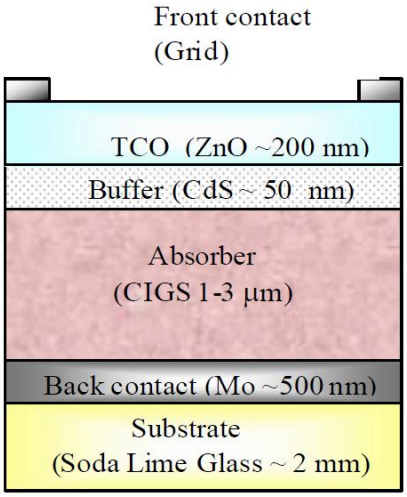

Figure 17. CIGS basic structure, from [25].

The cells are "grown" beginning with the substrate. Each additional layer is then deposited via various commercially available means. The numerous manufacturing techniques for fabricating CIGS cells are not investigated in this thesis but some of their limitations are taken into account.

1. Substrate

The substrate is the starting point for the manufacture of CIGS and is what determines whether the solar cell is flexible or rigid. Glass is the most common substrate used in production solar cells due to its low cost and ability to resist corrosion. Soda lime glass (SLG) is often used in manufacturing for its contribution to increasing performance properties. It has been shown that during the manufacturing process, sodium particles

from the substrate diffuse into the back contact layer and increase efficiency [26]. While this phenomenon is still being investigated, it has been proven that, all things being equal, cells manufactured on SLG have higher efficiency than other commonly used substrates.

The use of SLG as a substrate offers many benefits to CIGS solar cells but has one major drawback. Any glass substrate negates the ability of thin film cells to be light weight and flexible. Metals such as stainless steel or aluminum offer a suitable substrate that allow the solar cell to remain lightweight and flexible. Thin plastics and polymers can also be used as a viable replacement to SLG. As stated in [27], "Typical thickness of metal, polymer, or ceramic substrate materials is generally between 25 and 400 um, about one or two orders of magnitude lower than standard SLG substrates." By using certain metals as substrates, manufactures are able to retain the lightweight and flexible properties that are desired in CIGS cells.

2. Back Contact

The back contact of a solar cell is placed between the bottom of the absorber layer and the top of the substrate as seen in Figure 17. The back contact layer is designed to collect the carriers as they are produced in the absorber layer. The back contact in solar cells generally consists of a metal with low resistivity and serves as the positive lead or anode of the cell. For CIGS cells, molybdenum (Mo) is used for its compatibility in the manufacturing process [25].

3. Absorber Layer

The absorber or CIGS layer is where the majority of carrier generation is accomplished. CIGS is an I-III-VI semiconductor known as a chalcopyrite [1]. CIGS is an alloy of the materials $CuInSe_2$ (CIS) and $CuGaSe_2$ (CGS). Both CIS and CGS are direct band gap materials, with band gaps ranging from 1.07 eV to 1.76 eV and a high absorption coefficient. The range of band gap levels covers the infrared and higher energies of the sunlight spectrum. This results in most of the incident sunlight being absorbed close to the p-n hetero-junction formed with the CdS layer. This property is what allows the absorber layer to be manufactured in CIGS cells with thickness orders of magnitude smaller compared to traditional Si cells [25]. By alloying these two

compounds, we can vary the band gap of CIGS. This property of the CIGS system, and how they influence the solar cell operation, is covered in this chapter under section B.

4. Buffer Layer

The buffer layer is critical to the operation of the CIGS cell, providing the n-type junction layer in the solar cell hetero-junction. A thin layer of CdS is used in CIGS cells to accomplish this. CdS has a band gap of 2.4 eV, which allows most of the usable photons to pass through. Photons below wavelength 520 nm are absorbed by the CdS layer and contribute to losses [25]. It has been shown that a CdS thickness of 40-50 nm is ideal for commercially produced CIGS cells [2]. While the use of Cadmium is not preferred in manufacturing due to its toxic nature, a suitable replacement has not been found that can match its performance.

5. Window Layer

A window layer is designed to function in a similar fashion to the back contact. The window layer's purpose is to collect carriers as they are produced and transport them to the load. Since the window layer is on top of the solar cell, it needs to be transparent to the light spectrum that is required for photoelectric effect. To achieve this desired effect, a transparent conducting oxide (TCO) is often used for the window layer. A good TCO has a large enough band gap to allow a majority of photons to reach the absorber layer. It is also critical that the TCO has a low resistivity to reduce recombination losses. In common CIGS cells, zinc oxide (ZnO) is used for the TCO. ZnO has a band gap of 3.3 eV [25]. In this thesis, two layers of ZnO are used. The first layer, placed directly above the buffer layer, is a thin layer of iZnO. This aids in the cell bonding together in the manufacturing process. The second layer is ZnO doped with aluminum to give it low resistivity and increase efficiency [3].

B. ADJUSTING THE BAND GAP

Changing the band gap of a semiconductor changes what wavelengths of light can free an electron. This ability is needed to design a solar cell to be used in an environment

with a unique spectral irradiance. As stated earlier, CIGS is really an alloy between CIS and CGS. The correct representation of CIGS is

$$Cu(In_{1-x}, Ga_x)Se_2, \tag{4.1}$$

where x represents the mole fraction of Ga that is present in the alloy,

$$x = \frac{Ga}{(In + Ga)}. \tag{4.2}$$

An x value of zero represents pure CIS and has a band gap of 1.07 eV. An x value of one represents pure CGS with a band gap of 1.76 eV [1]. By varying x from zero to one, a manufacture can adjust the band gap of CIGS to the desired value. Adjusting the band gap according to the Ga content does not follow a linear trend. The equation relating band gap to mole fraction for intrinsic CIGS at 300 K is [28]

$$E_g = 0.02x^2 + 0.584x + 1.07. \tag{4.3}$$

From (4.3), the relationship between Ga content and band gap is slightly parabolic. This is due to the variation in size between the Ga and In elements when forming the chalcopyrite structure.

Band gap energy is related to photon wavelength by [16]

$$E_g(eV) = \frac{1.24}{\lambda(\mu m)} \tag{4.4}$$

where E_g is the band gap energy in electron volts and λ is the wavelength of light in micrometers. From (4.4), the relation between band gap and wavelength is inversely proportional. How higher band gap material can only effectively absorb shorter wavelength light is depicted in Figure 18.

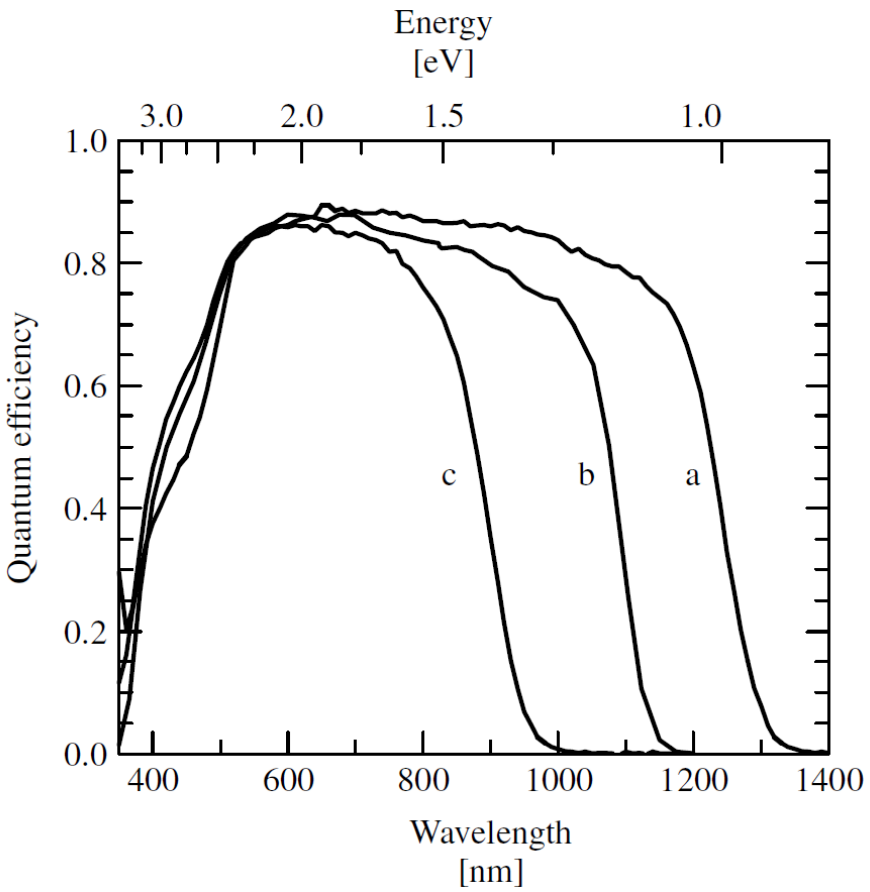

Figure 18. Quantum efficiency curves for CIGS solar cells with different relative Ga content giving band gaps of (a) 1.02 eV, (b) 1.16 eV, and (c) 1.4 eV, from [29].

Changing the band gap affects several performance parameters of solar cells. Cells with a higher band gap require high energy photons which in turn product higher energy electrons. The higher energy of each released electron causes the solar cell to have a higher V_{OC}. The drawback of high band gap material is that there are fewer usable photons entering the cell. The decrease of usable photons means that fewer electrons are produced which reduces the I_{SC}. The same logic can be applied to lower band gap cells. By allowing lower energy photons to create free electrons, the I_{SC} is increased while V_{OC} is decreased. Examples of current-voltage (IV) curves for CIGS cells with three different band gaps are displayed in Figure 19.

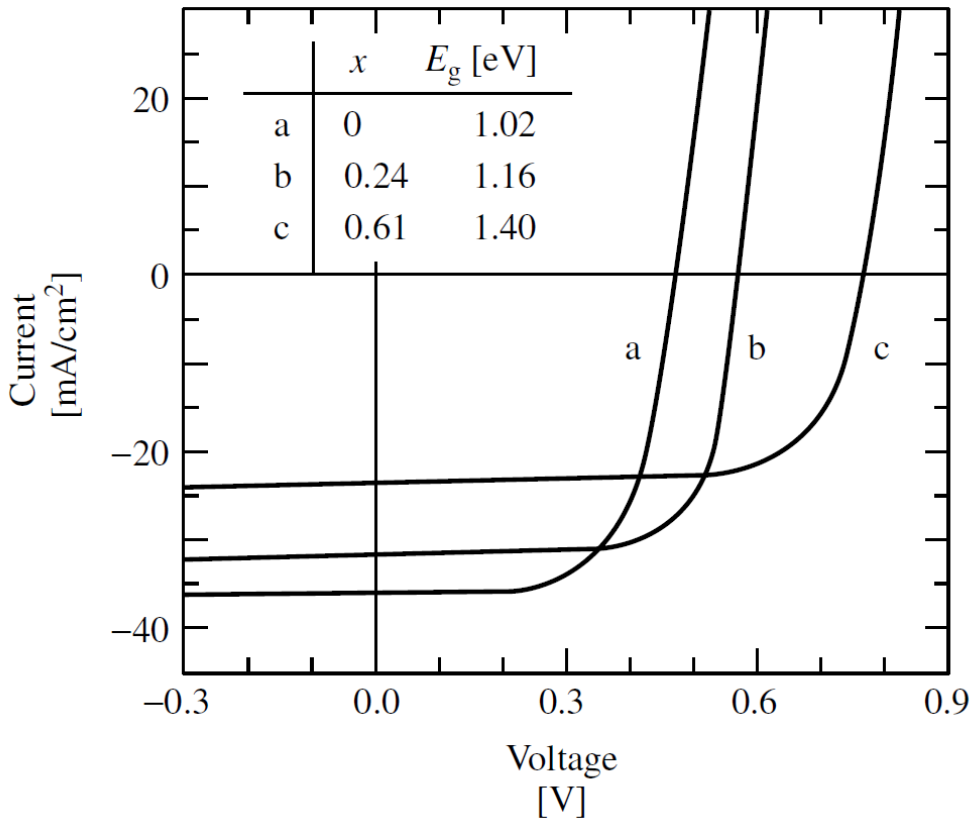

Figure 19. Current-voltage curves for CIGS solar cells with different relative Ga content giving band gaps of (a) 1.02 eV, (b) 1.16 eV, and (c) 1.4 eV, from [29].

C. BENEFITS OF CIGS CELLS MANUFACTURING

The use of CIGS solar cells has the potential to lead the market in thin film solar cells. This is due to the many benefits that CIGS cells offer both to the manufacturer and the consumer. As research continues into improving both the efficiency of the cells and reducing the manufacturing costs, CIGS cells have the potential to gain the majority of the thin film market share [30].

1. Inexpensive Manufacturing

One of the main benefits of CIGS cells is that they can be commercially manufactured at a fraction of the cost of traditional Si cells. To start with, crystalline Si cells need to be manufactured from extremely pure Si. Once a manufacturer has bulk Si with high enough purity, the material must be heated to extremely high temperatures for

it to form in a crystalline structure. This block of crystalline Si is then cut into wafers that must undergo numerous rounds of etching and doping before a final product is achieved [31]. This process is very time consuming and expensive for the manufacturer.

Thin film solar cells, such as CIGS can be produced in a much more efficient manner. The CIGS material can be deposited onto the substrate and back contact by a process called disposition. This essentially sputters the elements onto the substrate at high enough temperature to allow them to adhere. This process does not require the high tolerances of Si cells and is overall a more manufacture-friendly process [32]. In addition to the benefits of disposition, CIGS can be manufactured with a technique call roll-to-roll. Roll-to-roll manufacturing is displayed in Figure 20.

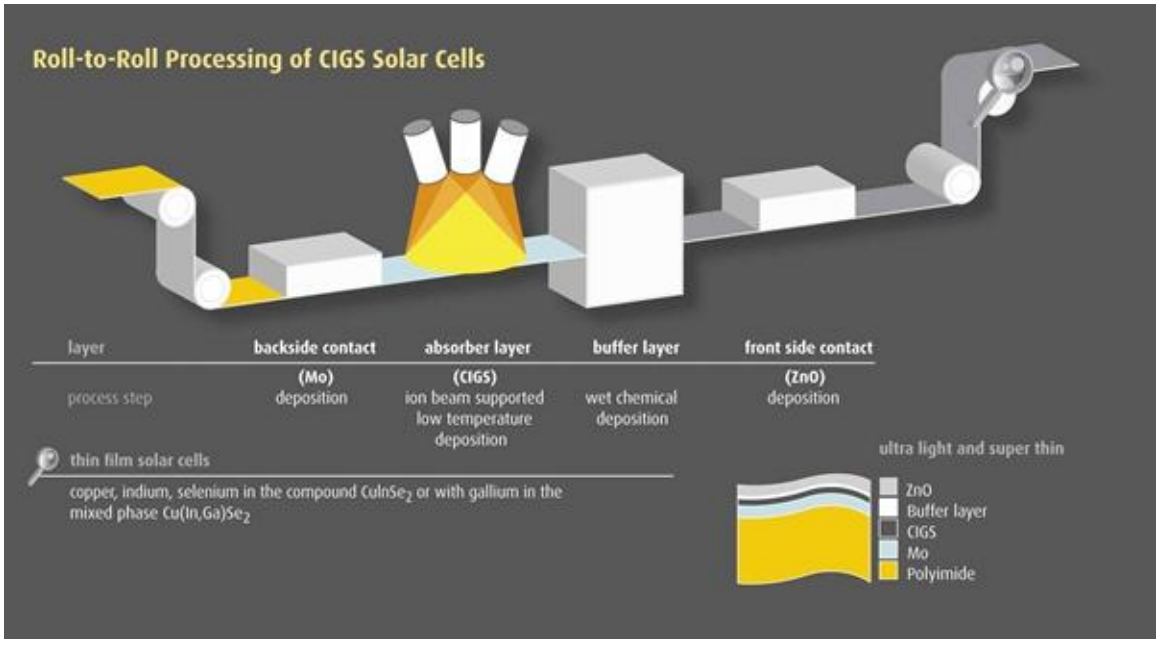

Figure 20. Roll-to-roll processing of CIGS solar cells, from [33].

With roll-to-roll manufacturing, companies can produce solar cells on a mass scale. As the flexible substrate is unrolled, it undergoes several processes that deposit layer upon layer onto the substrate. The process significantly cuts down on the production time but also allows for a continuous production cycle. Rather than cutting individual wafers of Si, roll-to-roll manufacturing supports a continuous sheet of solar cells being

produced. This process is so effective that it has allowed companies like Miasolé and Solibro to offer CIGS solar cells for a price point of $1/W [33].

2. Flexible

The flexibility of CIGS cells produced on a thin metal substrate is also a tremendous benefit. This flexibility gives CIGS an advantage over traditional Si cells with respect to mounting. A standard Si cell has properties consistent with a pane of glass. This makes a Si cell rigid and brittle, restricting the options for implementing solar arrays. The flexible nature of CIGS allows them to be mounted to structures that may not be perfectly flat. Research has shown the practicality of mounting CIGS cells on drone aircraft, thereby increasing their endurance [34].

3. Lightweight

A byproduct of being thin and flexible is also being lightweight. Being lightweight has its advantages for people who wish to take their solar cells with them as they travel about. This means that the market for solar cells will be able to increase from the traditional home or industrial power production to more expeditionary ones. CIGS cells could be marketed from campers, backpackers, and general outdoorsmen to beach goers and picnickers. Being lightweight give CIGS cells a portability that remains out of reach for Si based cells.

D. CURRENT STATE OF TECHNOLOGY.

Research into CIGS cells continues to improve the efficiencies seen in manufactured cells. The National Renewable Energy Laboratory's record efficiencies for numerous solar cell technologies versus the date that the efficiency was recorded is shown in Figure 21.

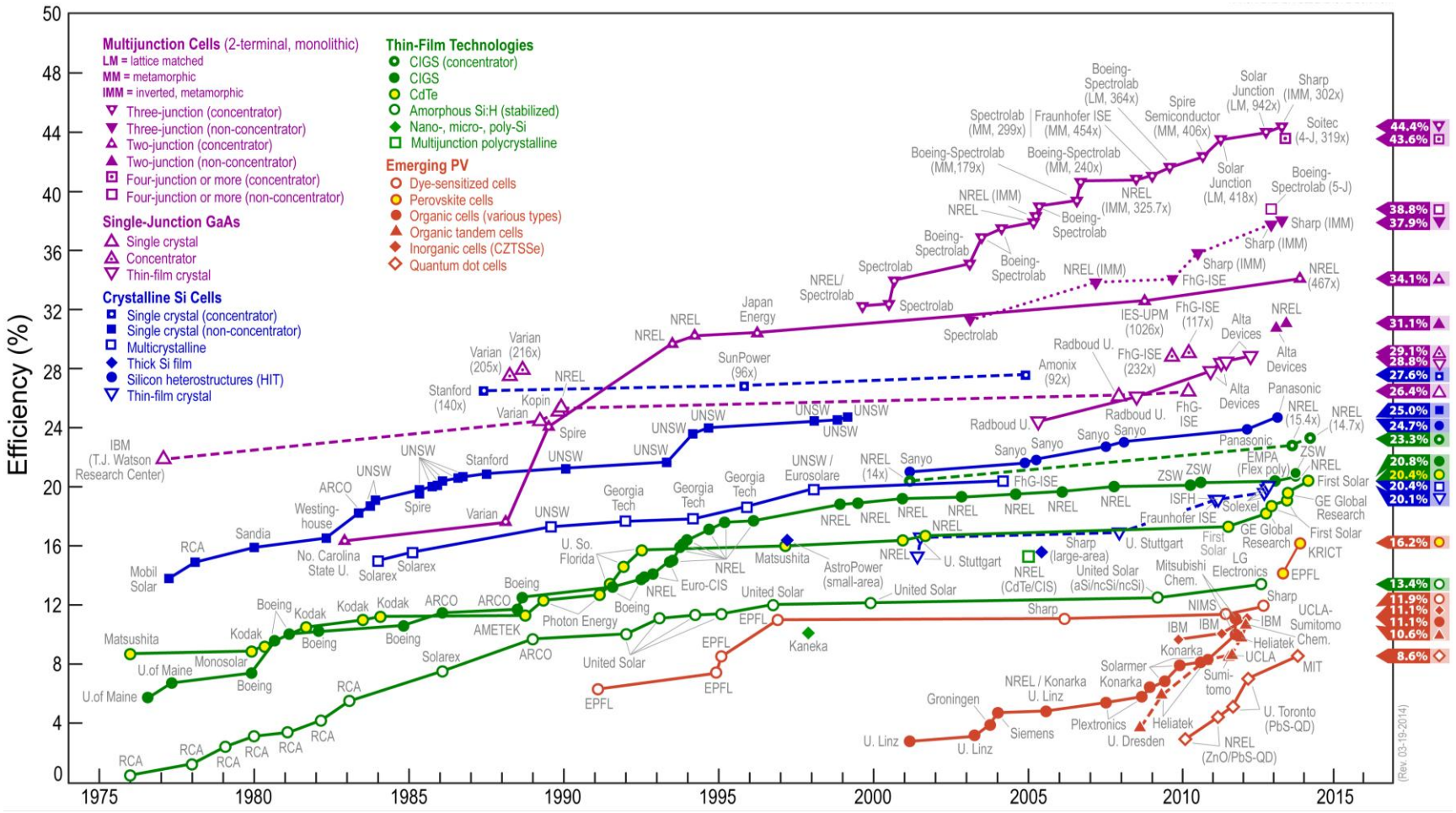

Figure 21. NREL's best research-cell efficiencies versus time, from [35].

Comparing CIGS cells performance in Figure 21 to other single junction non-concentrated cells, one can see that CIGS cells fall short. The current record for a CIGS cell is 20.8% efficiency, which leads the non-concentrated thin-film technologies. Compare this to a single crystal Si cell with an efficiency of 25.0% or a single crystal gallium arsenide cell with an efficiency of 26.4%, and CIGS cells are simply outpaced [35]. When consumers are looking to power their home with solar cells, efficiency is the driving factor. A cell that is light weight and flexible is of little concern if it has 5% lower efficiency. CIGS cells still have the advantage of being inexpensive. As manufacturers continue to improve the efficiency, CIGS will gain a larger foot hold on the market. While the industry standard is to measure cell efficiency against an irradiance of AM1.5, CIGS ability to have a variable band gap may give users in unique climates higher usable power than similar single junction cells. All these benefits point to an increase in CIGS demand with manufactures finding ways to increase efficiency and decrease production costs.

E. CONCLUSION

An in-depth look at CIGS solar cells was given in this chapter. The basic layers were discussed as well as the numerous benefits that CIGS possess over comparable cells. An explanation into how CIGS cells can be manufactured with various band gaps was given as well as the benefit that this offers to consumers. Finally, the current state of CIGS was discussed and compared to other solar cells that are on the market today.

V. SIMULATION AND RESULTS

A. SILVACO BASICS

Silvaco is a company that has specialized in many programs used for simulating engineering designs and testing them. More specifically, the ATLAS software provided by Silvaco is used to obtain the results discussed in this thesis. "Atlas provides general capabilities for physically-based two (2D) and three-dimensional (3D) simulation of semiconductor devices" [28]. ATLAS contains a comprehensive set of models and numeric integration techniques to accurately model semiconductor devices such as solar cells. The various inputs and outputs that ATLAS can accept and output are shown in Figure 22.

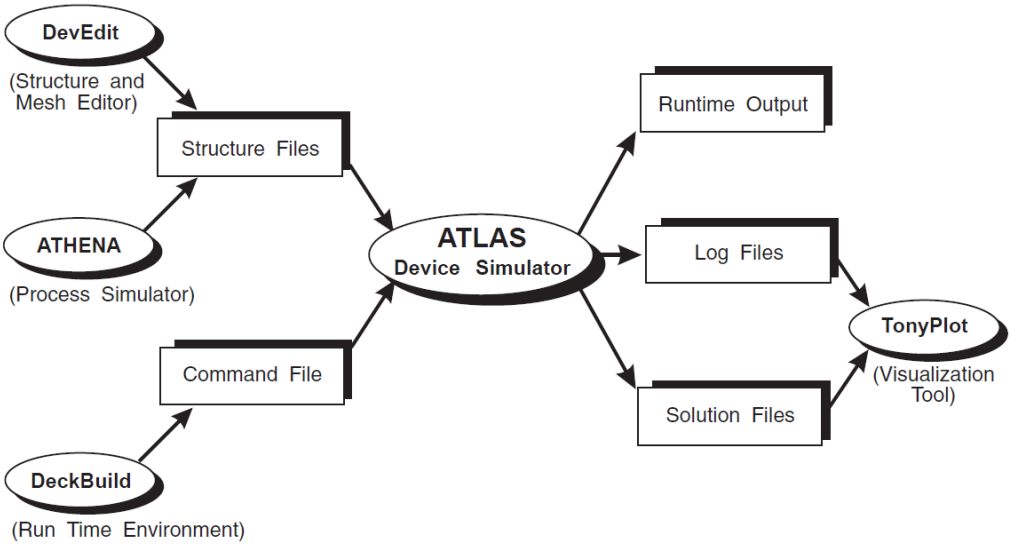

Figure 22. ATLAS inputs and outputs, from [28].

The basic format of ATLAS is to design a device using a grid of nodes. Several device parameters can be entered using various statements. ATLAS solves second order partial differential equations at each node to determine several characteristics of the device at equilibrium. These characteristics can include voltage, current, charge density, carrier concentration and so on. ATLAS solves these equations by using an iterative

method to attempt to converge on a solution. The art of using ATLAS is designing a grid that is fine enough to yield accurate results but not so fine that the simulation times out. A user can also encounter problems if their grid is so sparse as to not facilitate convergence of the model [28]. An in-depth look into the commands and functions used in ATLAS is available in Appendix A.

B. SOFTWARE CONFIRMATION

The first process of the simulation was to confirm the model against other documented CIGS cells and research. Confirming the model against experimental results is required in order to ensure that the model is feasible and realistic. Having a baseline or control cell is also critical with regard to optimization. By making only small changes to the confirmed cell, it can be inferred that the optimized cell still falls in the realm of a feasible and realistic solar cell.

Confirmation of the model against present day manufactured devices was desired; however, due to corporate competition, many companies are reluctant to freely advertise their proprietary knowledge and manufacturing techniques. A combination of several documented research works were used in the confirmation of this model [2] – [4].

1. Basic Cell Confirmation

For this thesis, a CIGS cell that was comprised of five layers was constructed. Starting with the top of the cell, the layers are as follows; ZnO-0.2 µm, iZnO-0.1 µm, CdS-0.05 µm, CIGS-2.0 µm, and Mo-0.4 µm. The simulated cell had a top area of one centimeter squared, based on the industry standard for laboratory testing. A visual representation of the base cell structure is depicted in Figure 23. For the coding used to create this model and additional parameters of the cell refer to Appendix B.

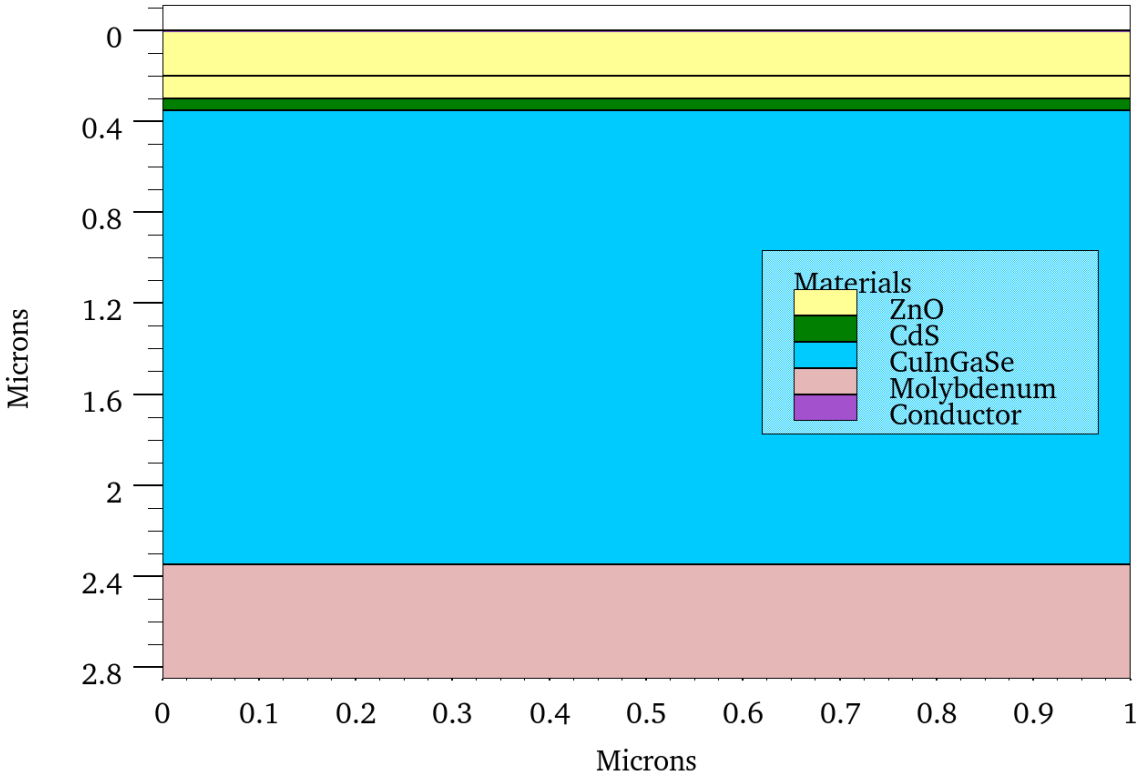

Figure 23. Control cells used as the basis of simulation.

In researching the basic semiconductor parameters for CIGS cells, it was found that the parameters varied only slightly. By not hard coding these parameters into ATLAS, the values were calculated automatically according to material parameters and doping. The semiconductor parameters used in this thesis were relative permittivity ε_r, band gap E_g, electron affinity χ_e, density of states in the conduction band N_c, density states in valence band N_v, electron band mobility μ_n, and hole band mobility μ_p. The values calculated by ATLAS are displayed in Table 1. These values come close to matching the values found in [36].

Table 1. Semiconductor material parameters.

	iZnO	CdS	CIGS
ε_r	8.49	10	13.6
E_g (eV)	3.37	2.48	varied
χ_e (eV)	4.5	4.18	4.58
N_c ($1/cm^3$)	$2.2x10^{18}$	$2.41x10^{18}$	$2.2x10^{18}$
N_v ($1/cm^3$)	$1.8x10^{19}$	$2.57x10^{19}$	$1.8x10^{19}$
μ_n (cm^2/Vs)	100	340	100
μ_p (cm^2/Vs)	25	50	10

The cell used as the base line was given a Ga content of 30%. This yielded a cell that had a band gap of 1.27 eV. After running the model it was determined that this cell had an efficiency of 17.13%. The efficiency measured from the model is consistent with cells of similar parameters.

2. Band Gap Confirmation

Continuing from the base cell, the method in which ATLAS calculated band gap needed to be verified. ATLAS allows the user to enter the mole fraction of Ga used in creating the CIGS region by the command *x.comp*. Five cells with different band gaps were modeled in this thesis. The amount of Ga used in the five cells was 10%, 30%, 50%, 70% and 90%. Each Ga content was entered separately and readings of ATLAS's calculated band gaps were taken. ATLAS's calculated band gaps from lowest to highest were 1.14 eV, 1.27 eV, 1.41 eV, 1.55 eV, and 1.69 eV. Performing a quadratic regression on this data yielded a band gap equation of

$$E_g(eV) = 0.024x^2 + 0.667x + 1.07 \tag{6.1}$$

where *x* is the mole fraction of Ga used in the CIGS region. An extrapolated curve of this data is shown in Figure 24.

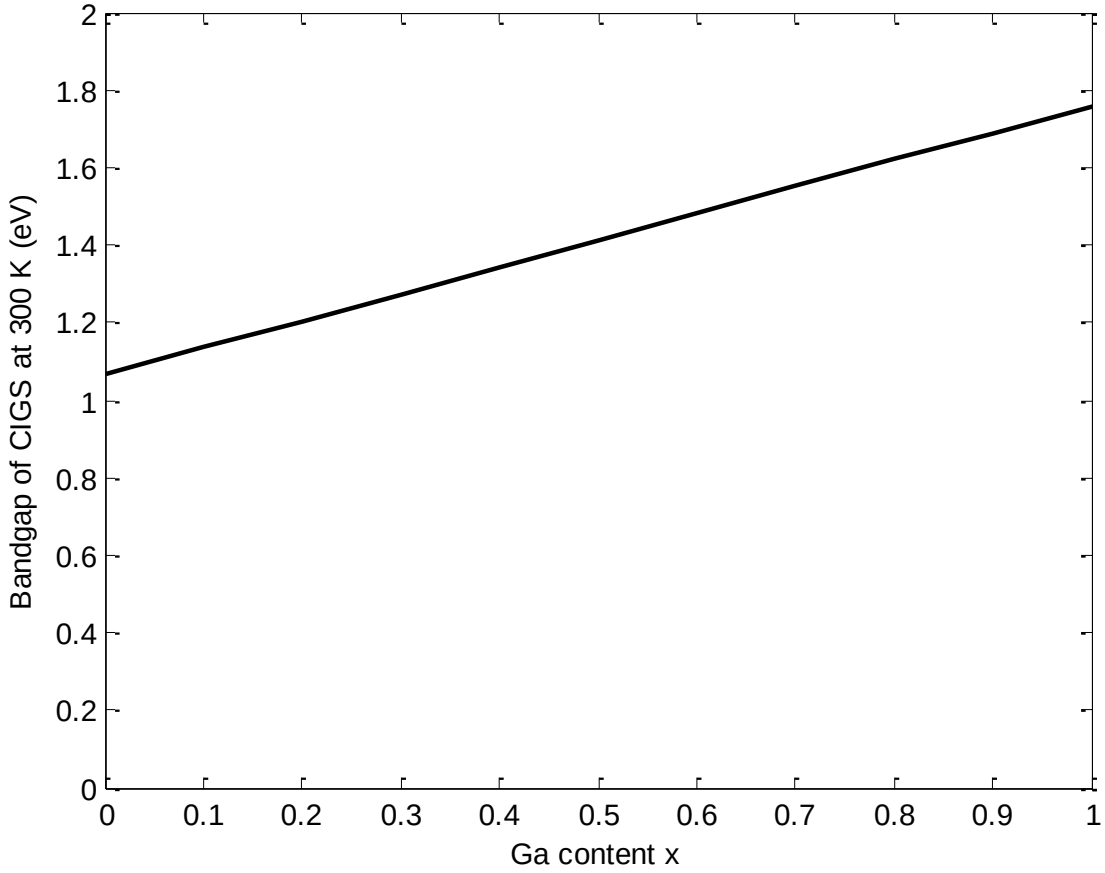

Figure 24. Extrapolated graph of Ga content versus band gap.

In addition to recording the calculated band gaps, IV curves for each of the five cells were created. Comparing the IV curves of cells with differing band gaps ensured that ATLAS was successfully modeling higher band gaps material. As stated in Chapter IV, higher band gap solar cells should produce a higher V_{OC} but a lower I_{SC}. The five IV curves of the control cell thicknesses are shown in Figure 25. A detailed breakdown of the data from Figure 25 is given in Table 2.

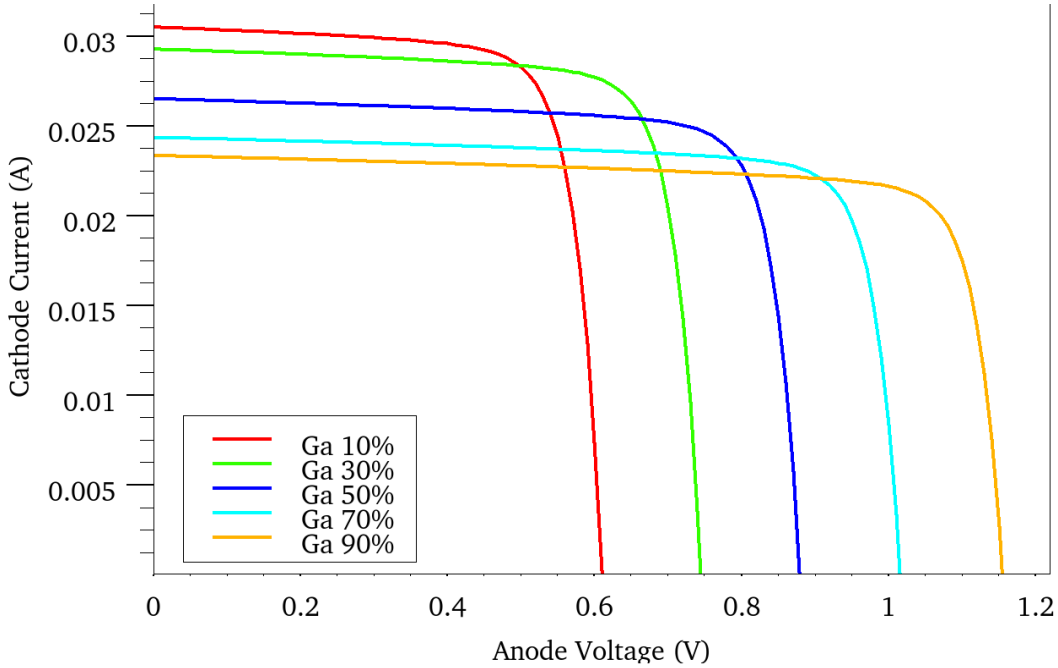

Figure 25. IV curves of the control cells with varying Ga content.

Table 2. Measurements from IV curves in Figure 25.

Ga content	0.1	0.3	0.5	0.7	0.9
I_{sc} (A)	0.0306	0.0293	0.0265	0.0244	0.0233
V_{oc} (V)	0.61	0.74	0.88	1.02	1.15
I_{max} (A)	0.0273	0.0268	0.0242	0.0223	0.0211
V_{max} (V)	0.52	0.64	0.77	0.90	1.04
P_{max} (W)	0.0143	0.0171	0.0186	0.0200	0.0219
Fill Factor	76.38%	78.64%	80.00%	81.08%	81.29%
Efficiency	14.25%	17.13%	18.63%	20.04%	21.90%
E_g (eV)	1.14	1.27	1.41	1.55	1.69

The final step to validate that ATLAS was correctly modeling the changing band gap was to produce a plot of the quantum efficiency of each cell. As the band gap of each cell increased, the wavelengths of light that could create an electron hole pair would decrease. This trait is depicted in Figure 26.

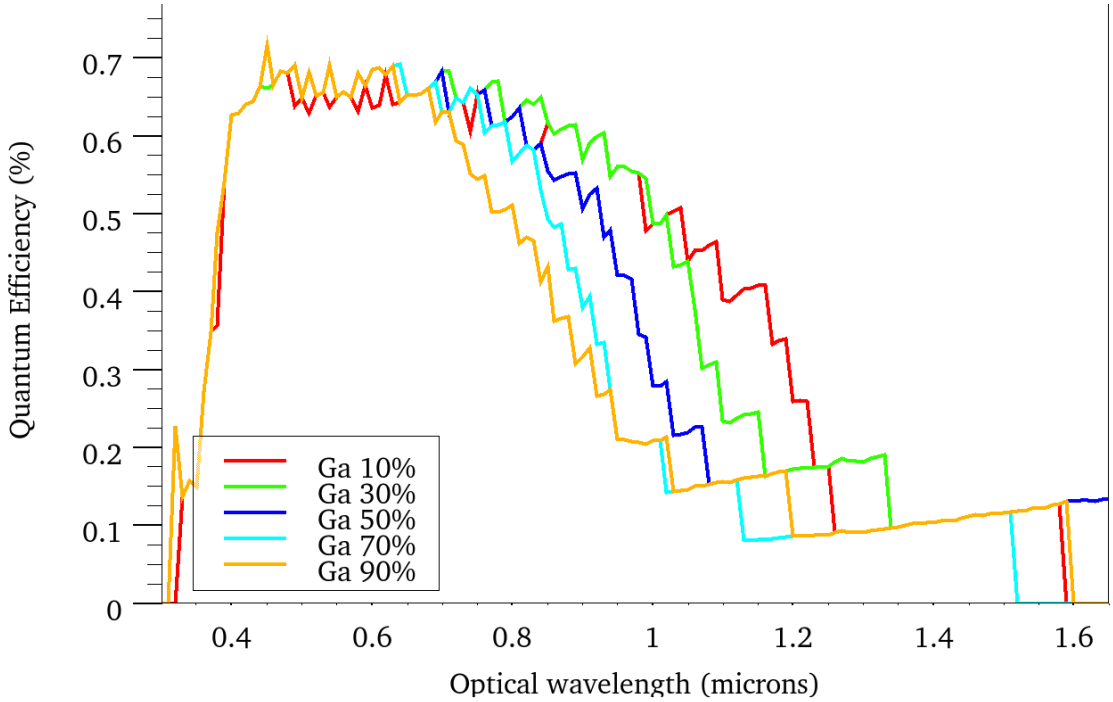

Figure 26. Quantum efficiency versus wavelength for CIGS cells with five different band gaps illuminated with AM0.

C. OPTIMIZATION

We sought to optimize the thicknesses for the layers of iZnO, CdS, and CIGS in each of the five band gap cells. The entire process to optimize a CIGS cell with a Ga content of 30% and a band gap of 1.27 eV is covered in this section. This band gap most closely mimics cells that are currently being produced. The same process was followed for the four remaining band gap cells. The optimization sweeps for these remaining cells can be found in Appendix C.

1. Individual Sweeps

Individual sweeps were first conducted by holding all variables constant and only varying the thickness of a single semiconductor layer. This allowed for the examination of how a CIGS cell reacts to variations of a single parameter.

The first step was to determine what range of values each semiconductor would be swept through. Current manufacturing limitations show that thicknesses below 0.05 µm are below the tolerances that are achievable. The lower limit for both iZnO and CdS

was set at 0.05 µm. The upper limit for these two layers was set at 0.1 µm thereby doubling the thickness. The CIGS layer was swept from 1.0 to 2.5 µm. Capping the CIGS layer at 2.5 µm ensures that the cell remains lightweight and flexible while attempting to achieve optimum efficiency.

The first individual sweep was that of iZnO and is displayed in Figure 27.

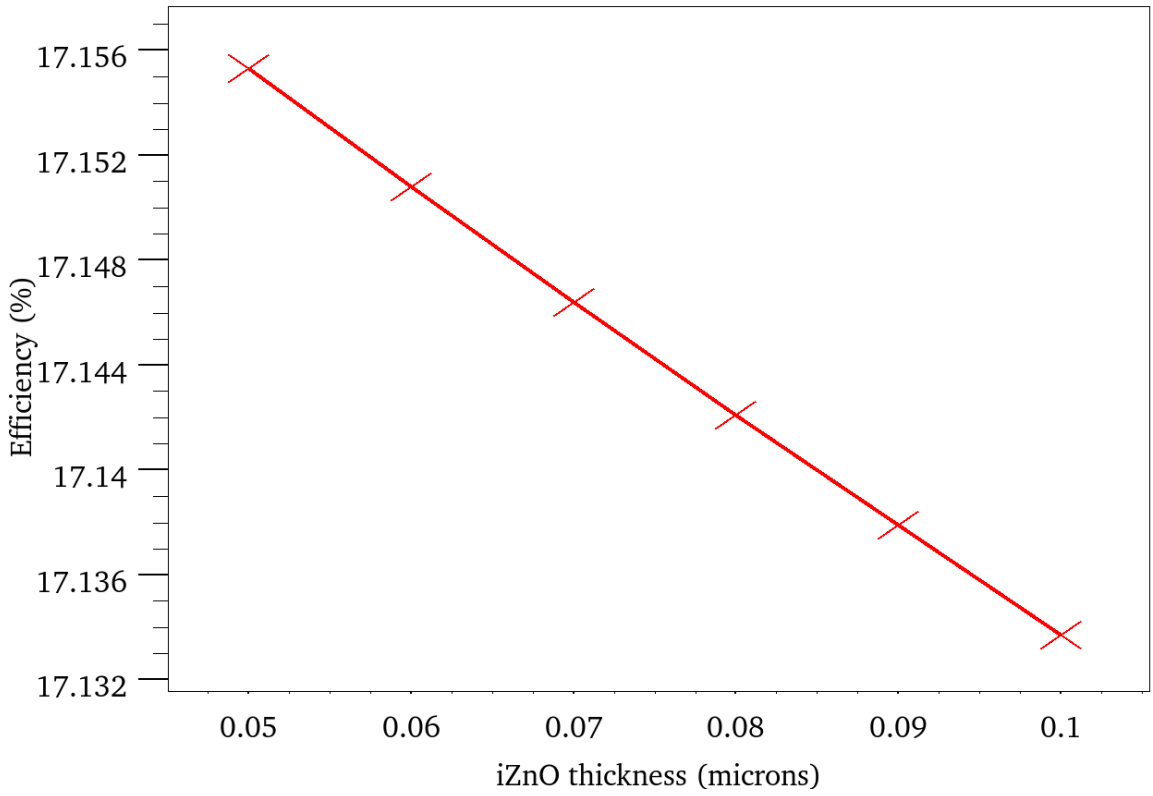

Figure 27. Sweep of iZnO thickness from 0.05 to 0.1 µm versus cell efficiency.

From Figure 27, it is evident that as the iZnO layer increases, the cell's efficiency decreases. The cell efficiency is not particularly sensitive to this change though. By doubling the iZnO layer, the efficiency only decreases by 0.02%. The cell is not sensitive to this change due to the fact that the iZnO layer is designed to aid in the bonding of the cell during the manufacturing and does not contribute to carrier generation.

The second individual sweep was that of CdS and is displayed in Figure 28.

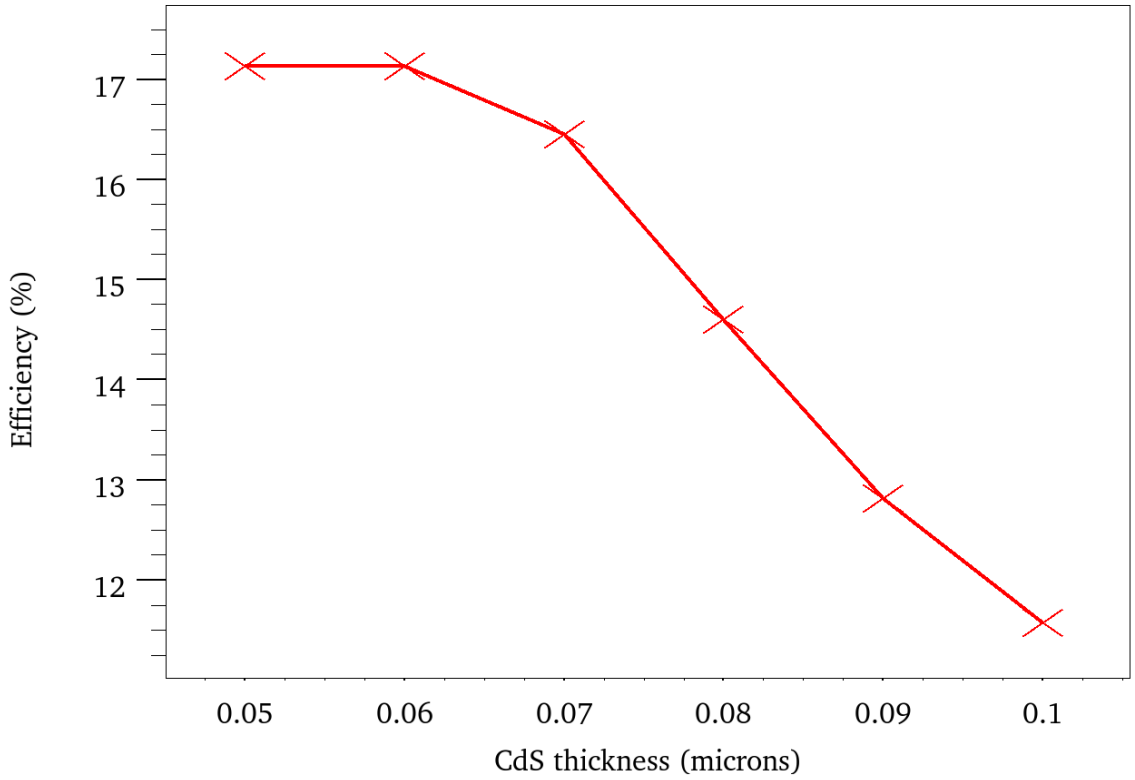

Figure 28. Sweep of CdS thickness from 0.05 to 0.1 µm versus cell efficiency.

The CIGS cell efficiency is significantly more sensitive to the CdS thickness. Cell efficiency fell over 5% by doubling the thickness of CdS. As stated previously, CdS has a band gap of 2.4 eV. Increasing the thickness CdS creates a stronger electric field between the p-n hetero-junction at the cost of absorbing more of the usable photons from reaching the CIGS layer. From Figure 28, CdS reached peak efficiency at 0.06 µm before efficiency began to fall off.

The final individual sweep was that of CIGS and is displayed in Figure 29.

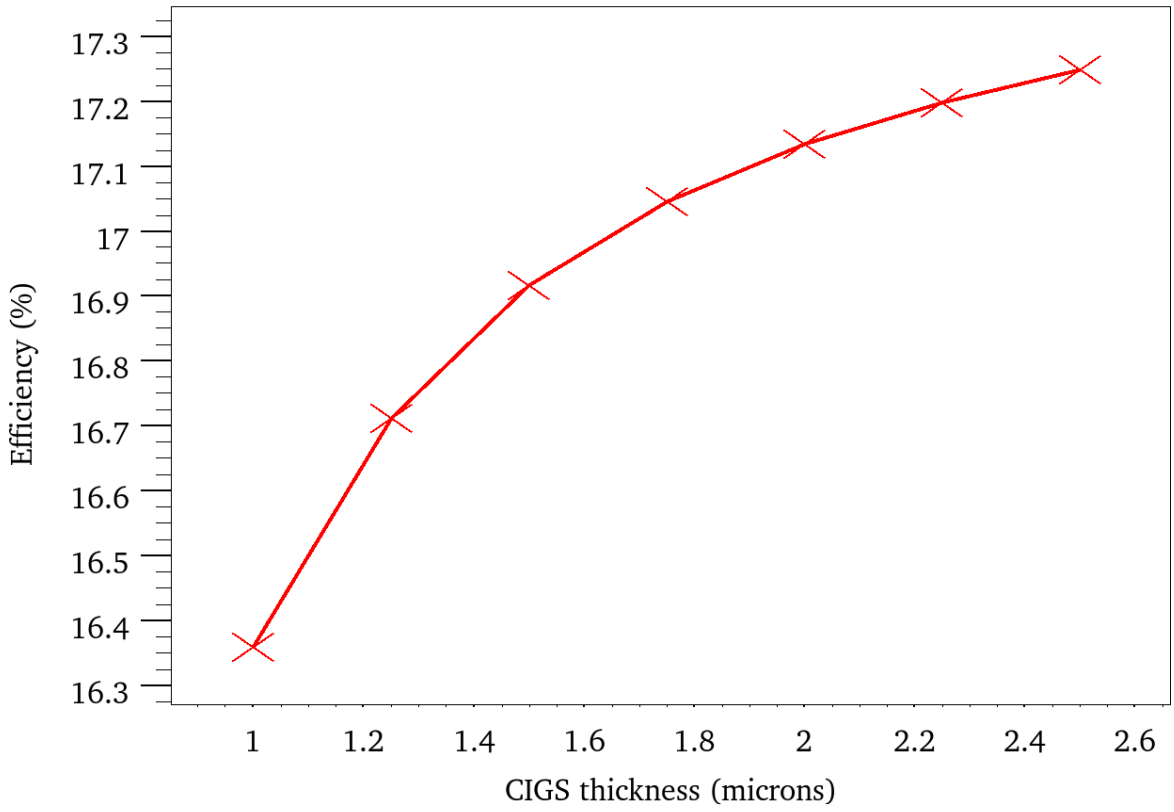

Figure 29. Sweep of CIGS thickness from 1.0 to 2.5 µm versus cell efficiency.

From Figure 29, is can be seen that cell efficiency continues to increase as the CIGS thickness increases. As the thickness of the absorber layer is increased, more carriers are generated. More carriers results in higher I_{SC} and a higher current at the maximum power point. As the CIGS layer increases, carriers generated farther from the p-n junction are subjected to a weaker electric field and more subject to recombination of electrons and holes. This recombination results in a law of diminishing returns where an increase of layer thickness does not result in major efficiency gains. The thickness of CIGS was capped at 2.5 µm to prevent chasing higher efficiency at the cost of losing the lightweight flexible qualities.

2. Combined Sweep

A combined sweep was required in order to evaluate how changing each layer affects the performance of the cell with regard to the others. Increasing a layer's thickness could result in shadowing a lower region and contribute to losses. To conduct

the combined sweep, thicknesses from each of the individual sweeps needed to be chosen. The two thicknesses from each semiconductor layer that yielded the highest efficiencies were kept. The optimization was run as three nested *for* loops, sweeping the thickness of iZnO first, then CdS, and finally CIGS. This resulted in a total of eight trial runs to determine the thicknesses of each layer that produces the optimum efficiency. Each trial run with corresponding thicknesses and the efficiency achieved is shown in Table 3. A visual representation of Table 3 with efficiency versus trial run is given in Figure 30.

Table 3. Optimization trial run with corresponding thicknesses and efficiency.

Trial Run	CIGS(μm)	CdS(μm)	iZnO(μm)	Efficiency
1	2.25	0.05	0.05	17.220%
2	2.25	0.05	0.06	17.216%
3	2.25	0.06	0.05	17.232%
4	2.25	0.06	0.06	17.219%
5	2.50	0.05	0.05	17.271%
6	2.50	0.05	0.06	17.267%
7	2.50	0.06	0.05	17.283%
8	2.50	0.06	0.06	17.270%

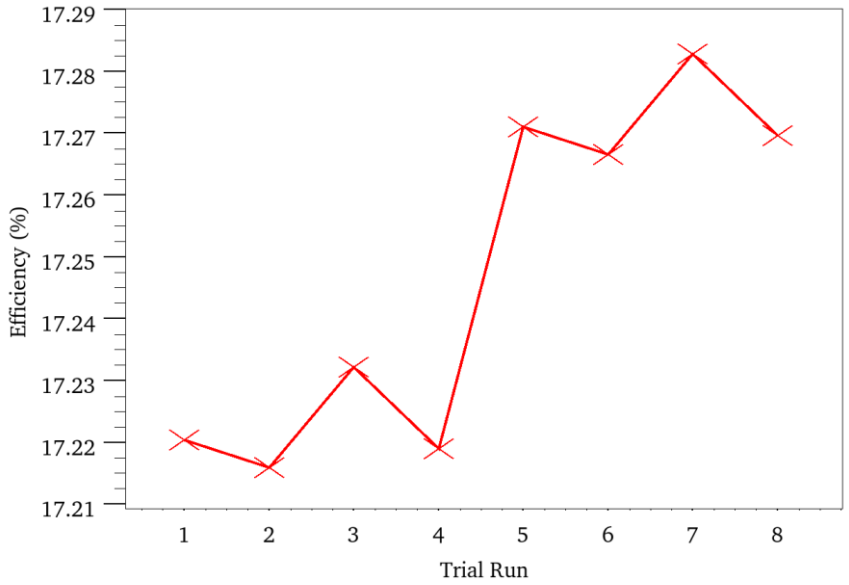

Figure 30. Optimization trial run versus cell efficiency.

From Figure 30 and Table 3, trial run seven achieved the peak efficiency of 17.283%. Trial run seven corresponded to an iZnO thickness of 0.05 µm, CdS thickness of 0.06 µm, and a CIGS thickness of 2.5 µm. Compared to the control cell with an efficiency of 17.13%, the optimized cell was able to achieve a 0.876% improvement in efficiency. The IV curves for both the control and optimized cell are displayed in Figure 31.

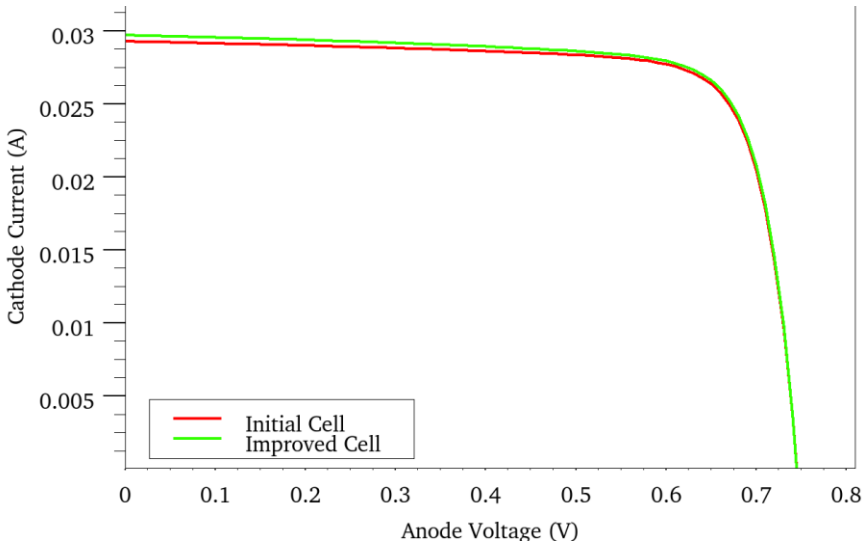

Figure 31. IV curves of Initial Cell and Optimized Cell.

D. FINAL RESULTS

The process described in the previous section was then repeated four times for the remaining cells and band gaps. Each of the individual sweeps exhibited the same trends as previously described. By following the same process, all of the cell's efficiencies were improved upon. A comparison of the control cell efficiency, the optimized cell efficiency, and the percent improvement achieved is shown in Table 4. From Table 4, the higher band gap cells achieved a larger efficiency increase than the lower band gap cells.

Table 4. Comparison of control cell efficiency with optimized cell efficiency.

Ga content	0.1	0.3	0.5	0.7	0.9
Band Gap (eV)	1.14	1.27	1.41	1.55	1.69
Control Cell	14.25%	17.13%	18.63%	20.04%	21.90%
Optimized Cell	14.31%	17.28%	18.89%	20.40%	22.40%
% Increase	0.421%	0.876%	1.396%	1.796%	2.283%

In optimizing the efficiency for each of the band gaps, it was found that the optimum thickness for each of the semiconductor layers remained the same. These thicknesses were 0.05 μm for iZnO, 0.06 μm for CdS, and 2.5 μm for CIGS. This was partially due to a limitation in ATLAS. The only solar spectrums that are preprogramed in ATLAS are AM0 and AM1.5, leading to each cell being illuminated with identical solar irradiance and no variation of the optimum points. Additional work is needed to input measured solar spectrums from various regions and climates on earth.

Although one optimum point was reached, this research was able to increase the efficiency of all five cells and show that an optimum band gap exists for a given spectrum. The optimized IV curves of all five cells are displayed in Figure 32, while detailed values corresponding to Figure 32 are displayed in Table 5.

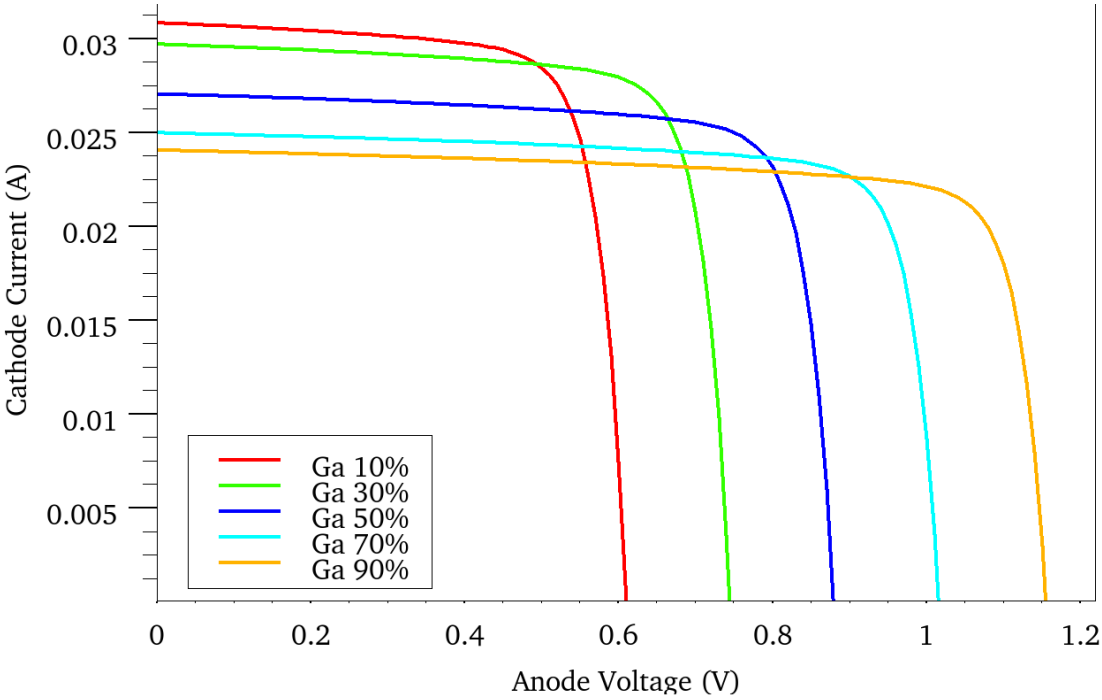

Figure 32. IV curves of the optimized cells with varying Ga content.

Table 5. Measurements from IV curves in Figure 32.

Ga content	0.1	0.3	0.5	0.7	0.9
I_{sc} (A)	0.0308	0.0297	0.0270	0.0250	0.0240
V_{oc} (V)	0.61	0.74	0.88	1.02	1.15
I_{max} (A)	0.0275	0.0270	0.0245	0.0227	0.0215
V_{max} (V)	0.52	0.64	0.77	0.90	1.04
P_{max} (W)	0.0143	0.0173	0.0189	0.0204	0.0224
Fill Factor	76.08%	78.22%	79.48%	80.49%	80.71%
Efficiency	14.31%	17.28%	18.89%	20.40%	22.40%
E_g (eV)	1.14	1.27	1.41	1.55	1.69

VI. CONCLUSION

A. CONCLUSION

The objective of this thesis was to design CIGS solar cells that were optimized for a specific climate or region. Silvaco ATLAS was used as a virtual fabrication and modeling tool. A base line cell was created by entering the parameters and characteristics of other known CIGS cells to verify the validity of the model.

Continuing from the base cell, four additional cells were created in which only the amount of Ga used in the creation of the CIGS layer was varied. This yielded a total of five cells that with band gaps of 1.14 eV, 1.27 eV, 1.41 eV, 1.55 eV, and 1.69 eV.

This research focused on optimizing the thicknesses of the semiconductor layers in each of the band gap cells. The semiconductor layers that were optimized were iZnO, CdS, and CIGS. For each of the band gaps, the three semiconductor layers were swept individually over a realistic range of thicknesses. Once the individual sweeps were complete, the two thicknesses that yielded the highest efficiency were kept. A combined sweep was then conducted with the two best thicknesses of each of the three layers. This resulted in a final optimization of eight trial runs. The highest efficiency was recorded along with the associated thicknesses of each of the semiconductor layers.

This simulation succeeded in increasing the efficiency of each cell. The largest band gap cell showed the greatest improvement with a control cell efficiency of 21.90% and an optimized cell efficiency of 22.40%. As solar cells approach higher and higher efficiency, the ability to continue to increase efficiency becomes increasing difficult. The control cell in this thesis was based on high efficiency CIGS cell; therefore, the efficiency improvement of the optimized cell represents a significant improvement. As previously stated, the current record efficiency for CIGS is 20.8% [35]. While the efficiency in this thesis is only theoretical, it exceeds the current record efficiency by 1.6%. Due to a limitation in ATLAS, only the solar spectrums of AM1.5 or AM0 could be used for this simulation. Nevertheless, the simulation did confirm that CIGS cells of varying band gaps responded differently to the spectrum of AM1.5.

B. RECOMMENDATIONS FOR FUTURE WORK

1. Physical Confirmation of Model

Confirmation of the model was an important step in this research; however, it is not a sufficient substitute to physical validation. CIGS cells with varying band gaps need to be produced and tested in contrasting geographic locations or solar irradiance to validate the concept presented in this thesis.

2. Model Improvement

Additional research is required in order to improve the ATLAS model used in this thesis. Research into how manufacturing defects affect the performance and how to model these characteristics will produce a more accurate model. Electron hole mobility and lifetime also need to be more accurately modeled for higher band gap CIGS material.

3. Currently Manufactured Cell Parameters

As stated before, current manufactures parameters for high efficient CIGS cells were not available. This is due to company's reluctance to freely publish parameters that required thousands of dollars and man hours to determine. By obtaining real world parameters, a more accurate model can be created and validated.

4. Additional Solar Spectrums

Designing solar cells that were specifically tuned to the solar irradiance of a region was the goal of this thesis. In order to fully validate this concept, additional solar irradiance profiles need to be entered into ATLAS. Currently, Silvaco and ATLAS contain the standard spectrums of AM0 and AM1.5. By entering measured solar irradiance into the model, a true optimum band gap cell can be developed and tested.

5. Higher Efficiency CIGS Concepts

With CIGS ability to vary band gap, differing designs could be tested in an attempt to achieve higher efficiency cells. A dual junction CIGS cell could be attempted by placing a higher band gap CIGS material above a lower band gap one. Another concept would be to design a CIGS layer that continually changed band gap with

thickness. The top of the CIGS layer would be high band gap material and then gradually transition to lower band gaps towards the bottom of the cell. This gradient could possess the benefits of a multi-junction cell without the need for tunnel junctions between layers of different materials.

THIS PAGE INTENTIONALLY LEFT BLANK

APPENDIX A. DEVICE BASIC CONSTRUCTION AND LAYOUT

To build a device in ATLAS from scratch, the user must use a program called DeckBuild. DeckBuild requires a very specific set of instructions to accurately design the device you wish to model. Both formatting and order matter when designing a device. There are five major categories that statements can fall under. Statements that specify the structure, material properties, numerical method for solving, statements to specify the solutions desired, and how to display the results. Within each of these categories are several statements used to finely tune each desired input parameter. A graphical depiction of major and minor statements in DeckBuild is displayed in Figure 33.

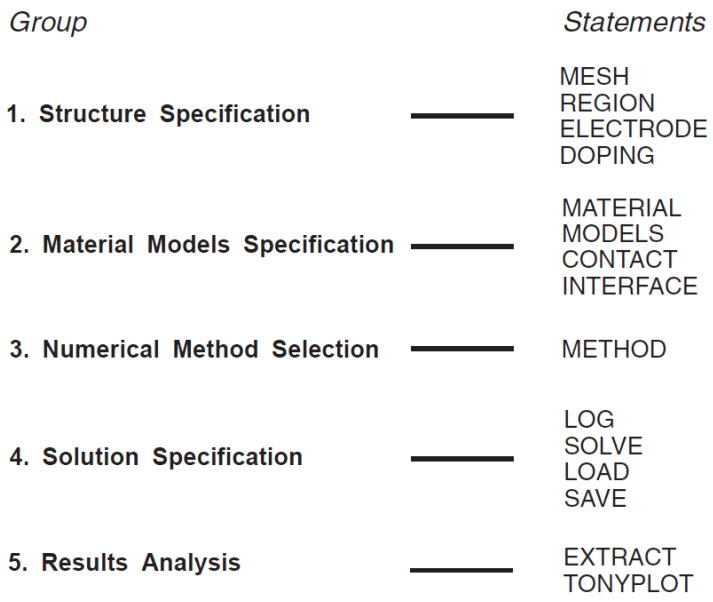

Figure 33. Categories of statement used in DeckBuild, from [28].

A. STRUCTURE SPECIFICATION

Under Structure Specification are several statements that allow the user to define the environment in which simulations will be run. These statements include Mesh, Region, Electrode, and Doping [28].

1. Mesh

The MESH statement is used to define the mesh of nodes that ATLAS will use during integration. The user can define *x* and *y* positions along with desired spacing between these locations. By defining the spacing between major locations, the user saves time from having to enter hundreds of *x* and *y* lines. For example, the following code creates 20 vertical lines from *x*= −1 to *x*= 1.

```
MESH AUTO WIDTH=10000

X.MESH LOCATION= −1.0 SPACING=0.1

X.MESH LOCATION= 1.0 SPACING=0.1
```

The results of this code with vertical grid lines every 0.1 µm are displayed in Figure 34.

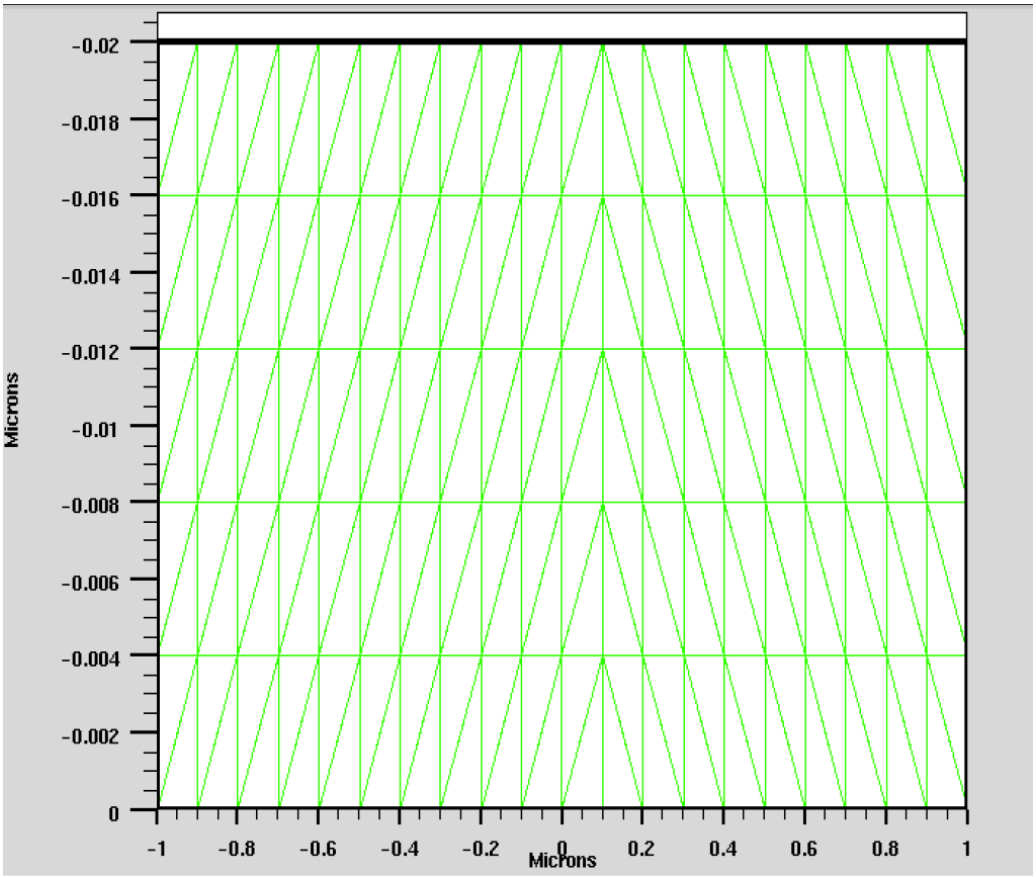

Figure 34. Mesh with vertical lines every 0.1 µm from *x*= −1 to *x*= 1.

ATLAS's primary method for creating and simulating devices is in two dimensions. The user can enter the statement *width* which mimics a three-dimensional device without additional calculations. For solar cells this means that the I_{SC} reflects a device with a top area defined by the user. A one centimeter squared cell, the industry standard for laboratory testing was simulated for this thesis.

The use of *auto* following the mesh statement is also a very useful tool provided by ATLAS. This command allows the user to skip specifying the *y* locations of the grid. ATLAS automatically defines these locations based on the layers and thicknesses of materials defined later. *Auto* was particularly useful in automatically creating the *y* mesh while sweeping various thicknesses [28].

2. Region

The REGION statement is used to fill the mesh with regions of material. Each region is assigned a number and material. The regions must also be bounded or defined in the mesh. Below is a structure of the region statement

REGION NUMBER=<integer> MATERIAL=<material type> <position>.

When using the *auto* meshing function of ATLAS, the position portion of the REGION statement consists of multiple parts. *Top* or *bottom* is used to define the position of the new layer with respect to the existing structure. ATLAS automatically places this new region either on the top or bottom of the stack. The thickness of the region must be defined next. When using the *auto* mesh function there are two ways to specify the *y* grid. The user can enter *ny* or *sy* at the end of the region statement to specify either the number of *y* lines or the spacing of the *y* lines, respectively. An example of auto meshing region statement is given below:

REGION number=1 material=CIGS thickness=2 top ny=10.

This statement places a CIGS layer of material on the top of the structure and define it as region one. This region has a thickness of 2 μm with ten gridlines in the *y* direction. The number defined in the region statement can be referenced through the remainder of the code [28].

3. Electrode

The ELECTRODE statement specifies the location and name of the electrodes being used. The electrodes can be bounded according to the mesh or can be placed along the top or bottom of the cell. The following statement defines the top of the structure as the cathode [28]:

ELECTRODE NAME=cathode top.

4. Doping

The DOPING statement is used to add dopants to the various regions of the structure. The DOPING statement can define the type of dopant, the distribution type, location, and the concentration [28]. An example of a doping statement is displayed:

DOPING uniform region=1 n.type concentration=1e17.

This statement specifies that region one, as defined in the REGION statement, will be uniformly doped with donor material to a concentration of 10^{17} per cm^3.

B. MATERIALS MODELS SPECIFICATION

The Material Models statements must follow the Structure Specification statements. In this section, the user can change various default material parameters and choose which physical model ATLAS uses during device simulation [28].

1. Material

The MATERIAL statement divides materials into three categories, semiconductors, conductors, and insulators. Each category has its own parameters that can be specified. For semiconductor materials, these parameters include band gap, permittivity, affinity, electron and hole mobility, and density of states [28]. An example of a material statement is given by:

MATERIAL MATERIAL=ZnO EG300=3.3 PERMITTIVITY=9 AFFINITY=4
MUN=100 MUP=25 NC300=2.2E18 NV300=1.8E19

2. Models

Physical models that the user desires to be present in the simulation are entered using the MODELS statement. ATLAS breaks physical models into five categories: mobility, recombination, carrier statistics, impact ionization, and tunneling [28]. Defining the recombination event as Shockley-Read-Hall (SRH) fixes the minority carrier lifetime to a predetermined value. ATLAS offers numerous additional model statements found in their manual [28].

C. NUMERIC METHOD SELECTION

The numeric method is where the user chooses how ATLAS solves for the device at equilibrium. ATLAS offers three choices for numeric method; NEWTON, GUMMEL, and BLOCK. The NEWTON method is used for systems that have a strongly coupled system of equations. NEWTON attempts to solve the system as a whole. This method always gives the best convergence but can be time consuming and requires a good initial estimate. The GUMMEL method is used when the system of equations are weakly coupled. GUMMEL attempts to solve each unknown individually while keeping other variables constant. This yields the shortest calculation time but can become unstable if applied to the wrong system. The BLOCK method is a combination of the previous two, solving some equations as coupled while others are de-coupled. For this research, the NEWTON method was used in order to ensure that the system converged [28].

D. SOLUTION SPECIFICATION

Once all parameters of the device have been defined and the numeric method specified, the user can enter the solution specification. The solution specification section allows the user to extract the data required from the device. ATLAS initializes each device with a zero bias on all the electrodes. The standard operation for this step is to have the user define the voltages at each of the conducting nodes. ATLAS then calculates the current through the electrodes as well as internal electric fields [28].

1. Log

Log files are used when only the terminal characteristics of a device are desired. The log file will store voltage and current of each electrode in DC simulations. The user specifies the command:

LOG OUTFILE=<FILENAME>.log

to open a log file with the name as defined by the user. The SOLVE statement that follows inputs all the recorded electrode data into this log file.

2. Solve

The SOLVE statement is where the user defines what voltages to sweep the device with. As stated previously, ATLAS initializes the device at zero bias on all electrodes. Using the SOLVE statement, the user can specify the final voltage to sweep to as well as the voltage step size. An example of a SOLVE statement is given by:

SOLVE VSTEP=0.01 VFINAL=1.3 NAME=anode.

This SOLVE statement sweeps the voltage on the anode from 0 V to 1.3 V in increments of 0.01 V [28].

3. Load

The LOAD statement loads a previously saved file into DeckBuild. Loading a previous file can help with the initial guess that ATLAS must perform of the device or can allow the user to compare results of a previous simulation to the current simulation. Files are loaded into DeckBuild using:

LOAD INFILE=<FILENAME>.

4. Save

The SAVE statement allows the user to save all node point information to an outfile [28]. Unlike the LOG statement that records only the terminal characteristics of a device, the SAVE statement records all the device parameters such as the mesh, materials, and doping. Since SAVE statements record every detail of the device, they take

up much more memory than a LOG statement. The command for using a SAVE statement is:

SAVE OUTFILE=<FILENAME>.str.

E. RESULTS ANALYSIS

The results analysis statements allow the user to visually display details of the device. There are two commands that enable the user to do this, the EXTRACT command and the TONYPLOT command. The EXTRACT statement allows for the user to define which device parameters they specifically desire and how to calculate them. For this thesis, seven EXTRACT statements were used to solve for I_{SC}, V_{OC}, maximum power current, maximum power voltage, maximum power, fill factor, and efficiency. An example of an EXTRACT statement is:

EXTRACT NAME="Short Circuit Current" max(i."cathode").

This statement finds the maximum current at the cathode and stores the value in the name "Short Circuit Current."

TONYPLOT is a separate command used to visually display the data of any saved file. For solar cells, we are mostly concerned with analyzing the IV curves, so TONYPLOT is most often used to display log files [28]. An example of the TONYPLOT command is given by:

TONYPLOT <FILENAME>.log.

THIS PAGE INTENTIONALLY LEFT BLANK

APPENDIX B. ATLAS SOURCE CODE

A. BASELINE CIGS CELL FILE

```
go atlas

#DEFINE THE VARIABLE TO SWEEP
set iZnO_thick=0.1
set CdS_thick=0.05
set CIGS_thick=2.0

# DEFINING THE MESH (1cm2)
mesh auto width=1e8
x.mesh location=0.0 spacing=0.5
x.mesh location=0.5 spacing=0.5
x.mesh location=1.0 spacing=0.5

# REGIONS
region num=1 material=ZnO  bottom thick=0.2               ny=50 conductor
region num=2 material=ZnO  bottom thick=$iZnO_thick  ny=50
region num=3 material=CdS  bottom thick=$CdS_thick    ny=50
region num=4 material=CIGS bottom thick=$CIGS_thick ny=350 x.comp=0.3
region num=5 material=Molybdinum bottom thick=0.4      ny=100 conductor

# ELECTRODES
elec num=1 name=cathode top
elec num=2 name=anode   bottom

# DOPING
doping uniform region=1 n.type concentration=1e18
doping uniform region=2 n.type concentration=1e18
doping uniform region=3 n.type concentration=1e17
doping uniform region=4 p.type concentration=2e16

# MATERIAL PROPERTIES
material TAUN=1e-7 TAUP=1e-7 COPT=1.5e-10 AUGN=8.3e-32 AUGP=1.8e-31

material region=1 resistivity=167
material region=5 material=Molybdinum resistivity=0.055

trap material=CIGS donor e.level=0.635 sign=5e-13 sigp=1e-15 \
density=1e14 y.max=2.32 degen.fac=1
trap material=CdS acceptor e.level=1.2 sign=1e-17 sigp=1e-12 \
density=1e18 y.min=0.33 degen.fac=1
```

```
# MODELS
models srh temperature=300 bound.trap

# SOLAR LIGHT (AM 1.5)
beam num=1 x.origin=0.5 y.origin=-1 am1.5 wavel.start=0.285 \
wavel.end=1.655 wavel.num=137

# SOLVE I-V CURVE
solve init
solve previous
solve b1=1
log outfile=CIGS_init.log
solve previous

extract name="Short Circuit current" max(i."cathode")
solve vstep=0.01 vfinal=1.3 name=anode \
compliance=$"Short Circuit current" cname=cathode

#PLOT THE RESULTS (anode voltage vs. cathode current)
tonyplot CIGS_init.log –set IV.set

#EXTRACT ADDITIONAL PARAMETERS
extract name="Open Circuit Voltage" x.val from curve (v."anode", i."cathode") \
    where y.val=0
extract name="Max Power Current" x.val from
curve(i."cathode",((v."anode")*(i."cathode"))) \
    where y.val=max((i."cathode")*(v."anode"))
extract name="Max Power Voltage" x.val from
curve(v."anode",((v."anode")*(i."cathode"))) \
    where y.val=max((i."cathode")*(v."anode"))
extract name="Max Power" max((i."cathode")*(v."anode"))
extract name="FF1" $"Max Power"/($"Short Circuit Current"*$"Open Circuit Voltage")
extract name="Eff1" $"Max Power"/0.001

quit
```

B. CIGS CELL SWEEP FILE

```
go internal

#LOAD THE FILE TO SWEEP
load infile=”cellstructure”.in

#DETERMINE WHERE TO SAVE THE FILE
```

```
save type=sdb outfile=sweep.dat

#SWEEP THE PARAMETERS
sweep parameter=iZnO_thick type=linear range=”0.05,0.06,2” \
parameter=CdS_thick type=linear range=”0.05,0.06,2” \
parameter=CIGS_thick type=linear range=”2.25,2.5,2”

endsave

#PLOT THE RESULTS
tonyplot sweep.dat

quit
```

THIS PAGE INTENTIONALLY LEFT BLANK

APPENDIX C. ADDITIONAL BAND GAP CELL RESULTS

A. GALLIUM OF 10% WITH BAND GAP OF 1.14 eV

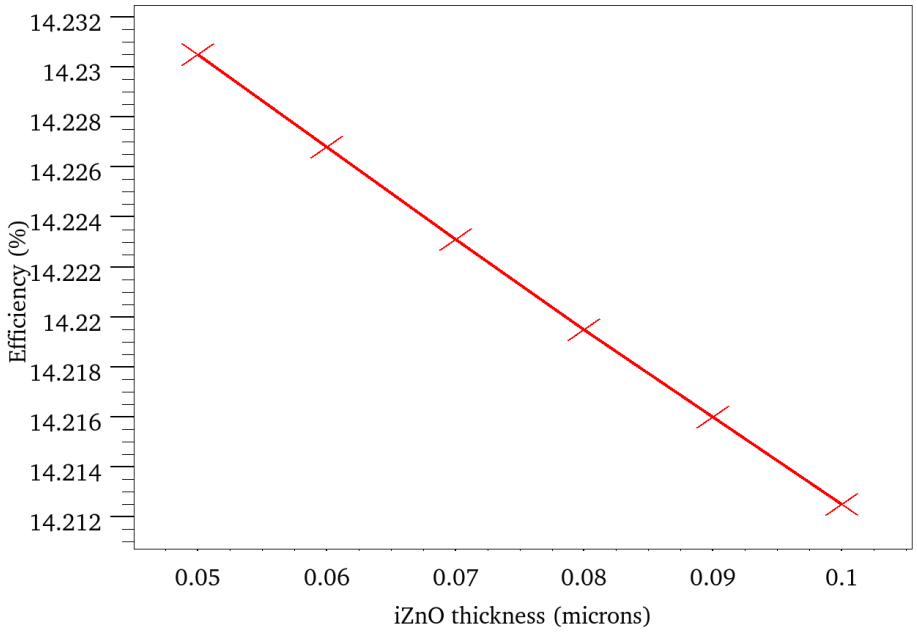

Figure 35. Sweep of iZnO thickness from 0.05 to 0.1 µm versus cell efficiency.

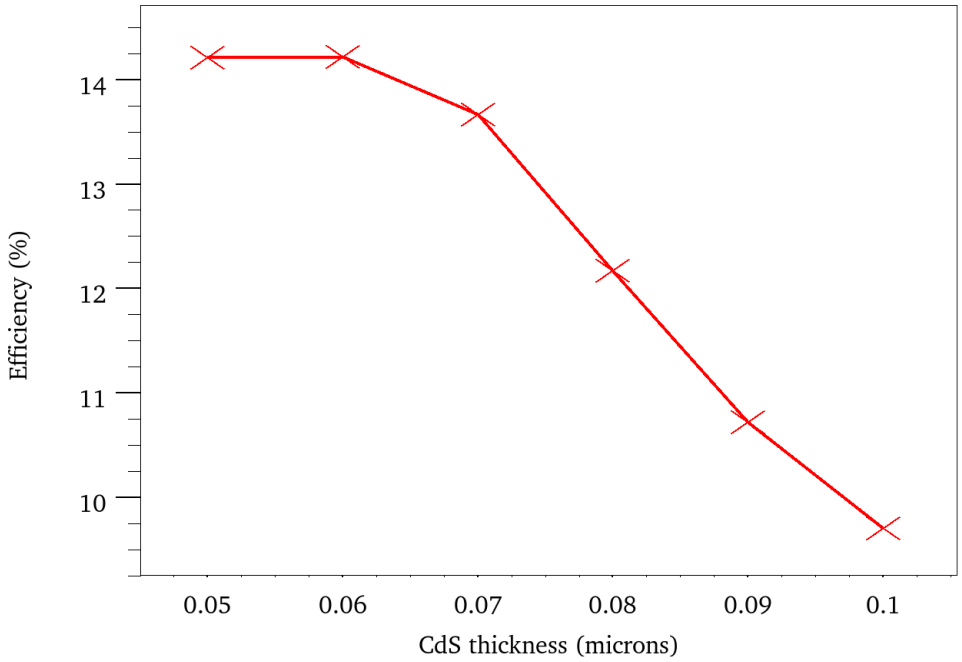

Figure 36. Sweep of CdS thickness from 0.05 to 0.1 µm versus cell efficiency.

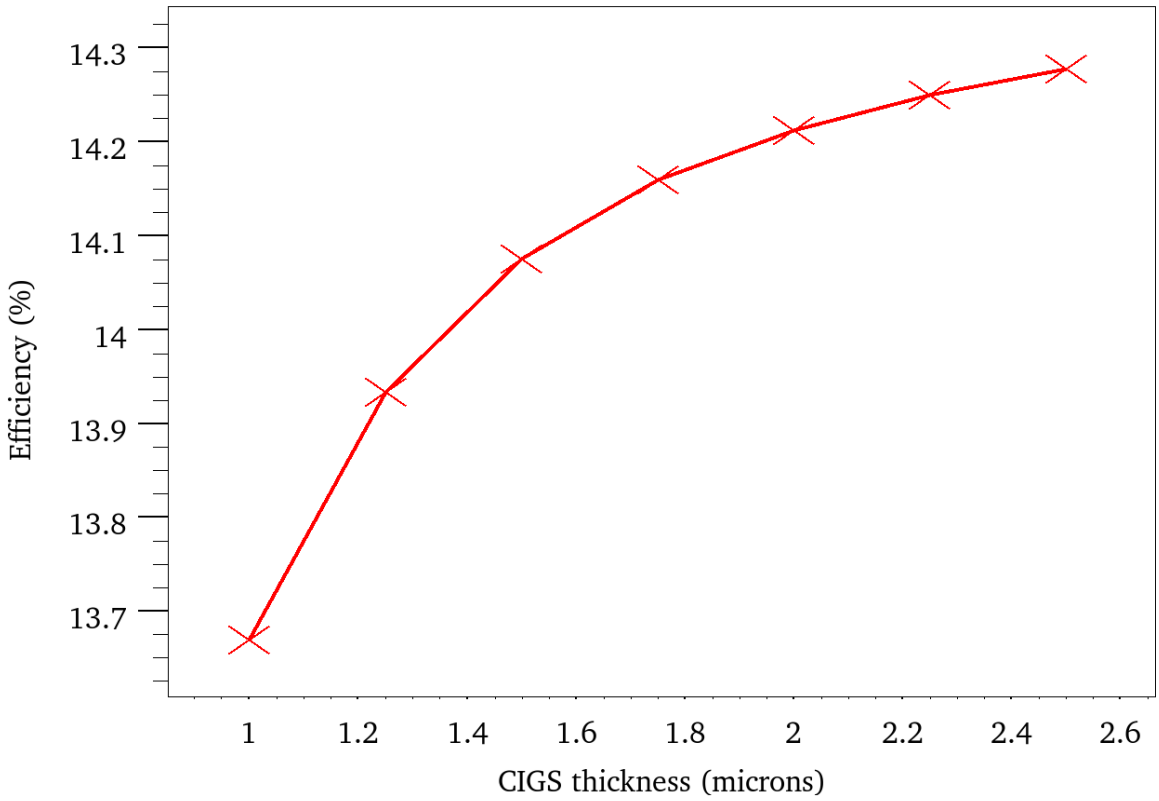

Figure 37. Sweep of CIGS thickness from 1.0 to 2.5 µm versus cell efficiency.

Table 6. Optimization trial run with corresponding thicknesses and efficiency.

Trial Run	CIGS(µm)	CdS(µm)	iZnO(µm)	Efficiency
1	2.25	0.05	0.05	14.268%
2	2.25	0.05	0.06	14.264%
3	2.25	0.06	0.05	14.282%
4	2.25	0.06	0.06	14.272%
5	2.50	0.05	0.05	14.296%
6	2.50	0.05	0.06	14.292%
7	2.50	0.06	0.05	14.310%
8	2.50	0.06	0.06	14.300%

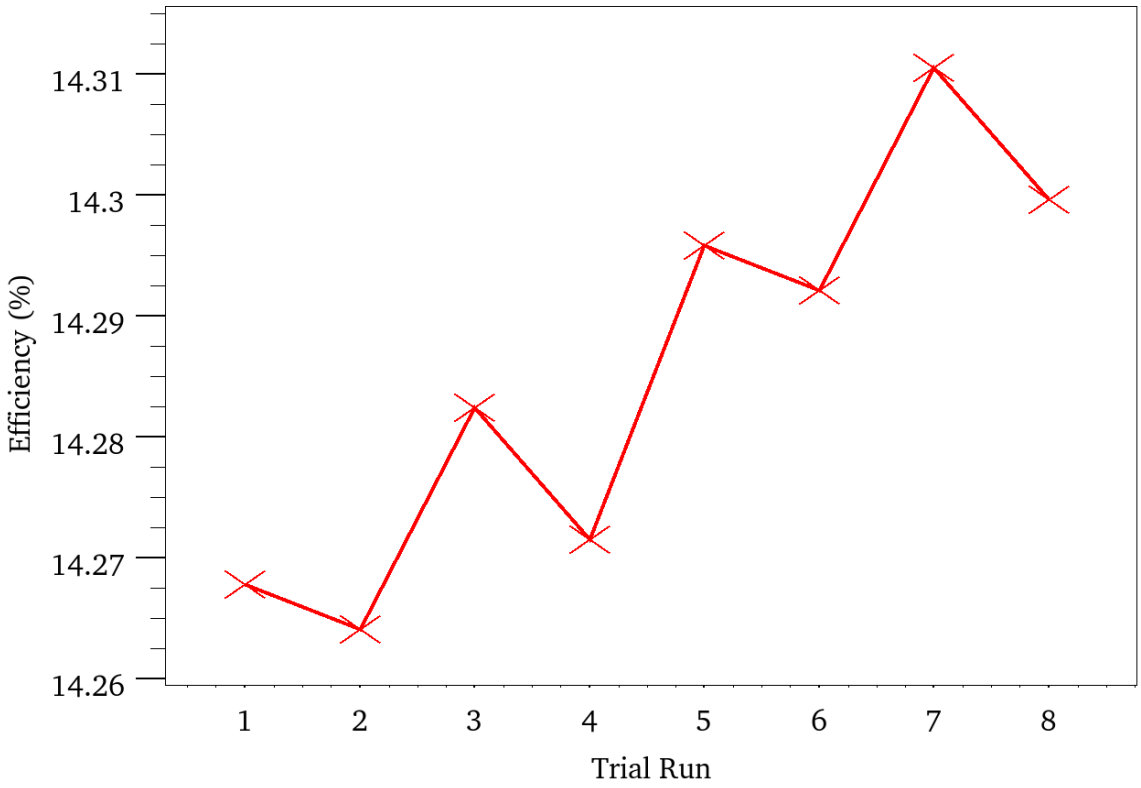

Figure 38. Optimization trial run from Table 6 versus cell efficiency.

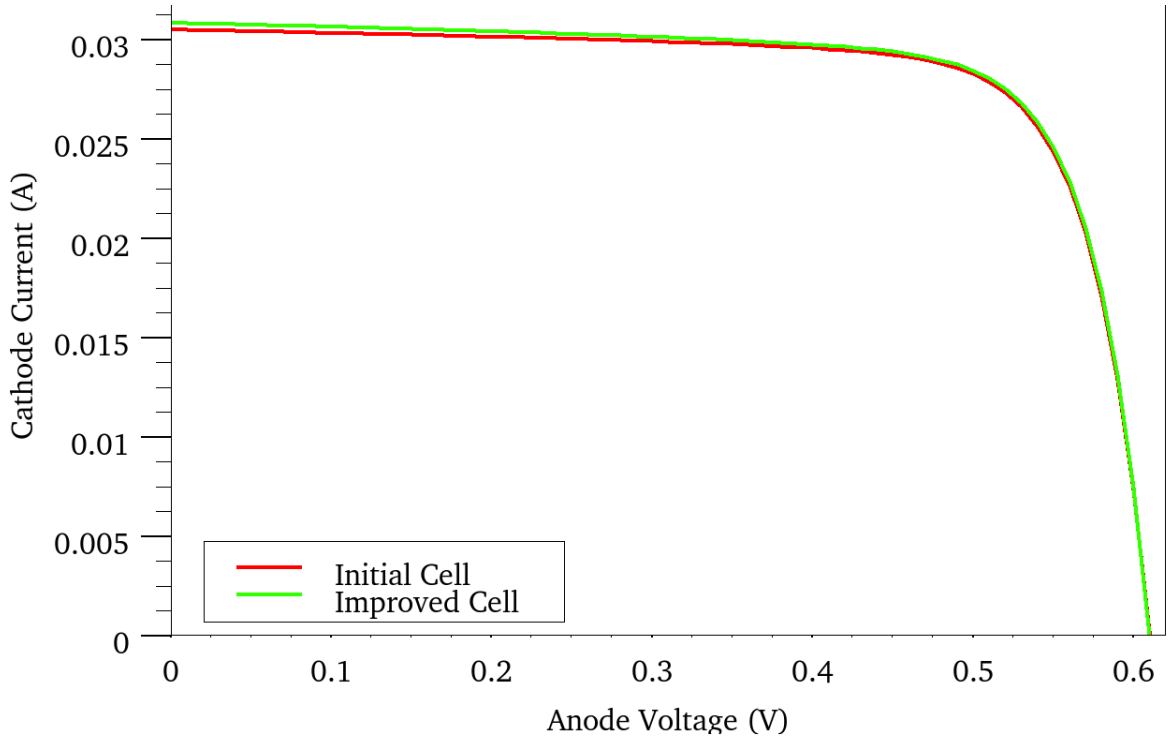

Figure 39. IV curves of initial cell and optimized cell.

B. GALLIUM OF 50% WITH BAND GAP OF 1.41 eV

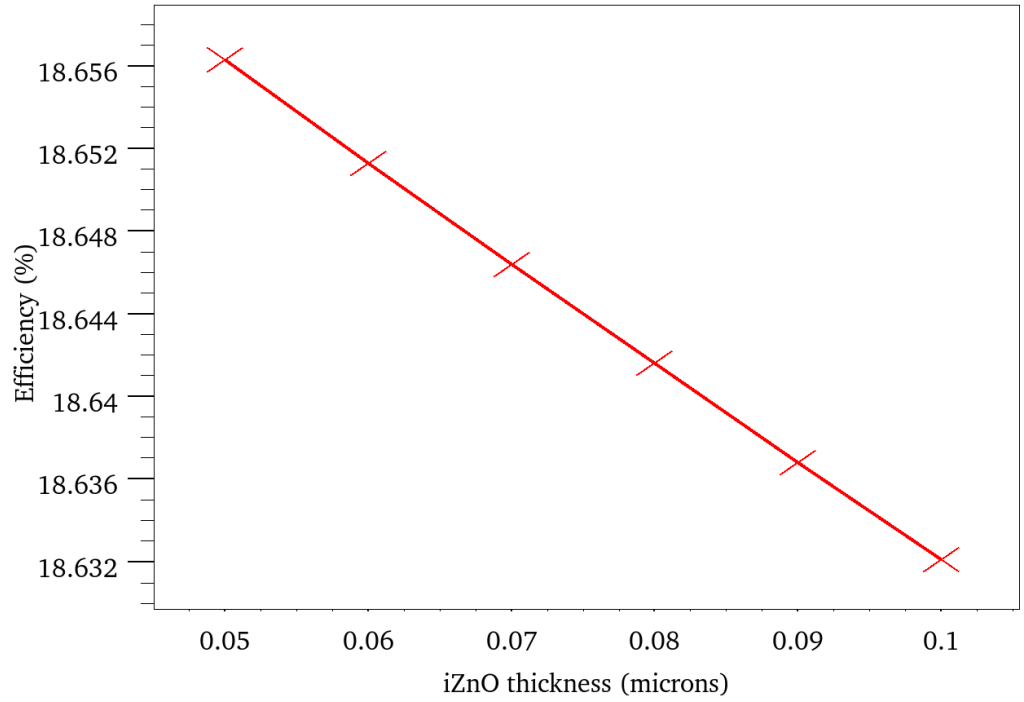

Figure 40. Sweep of iZnO thickness from 0.05 to 0.1 µm versus cell efficiency.

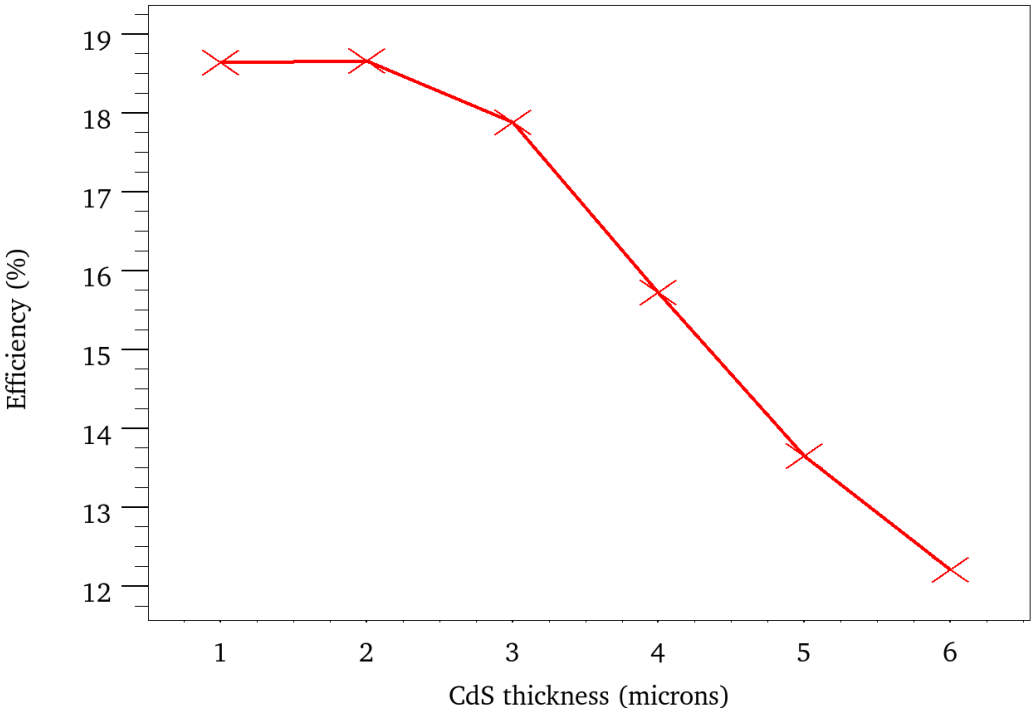

Figure 41. Sweep of CdS thickness from 0.05 to 0.1 µm versus cell efficiency.

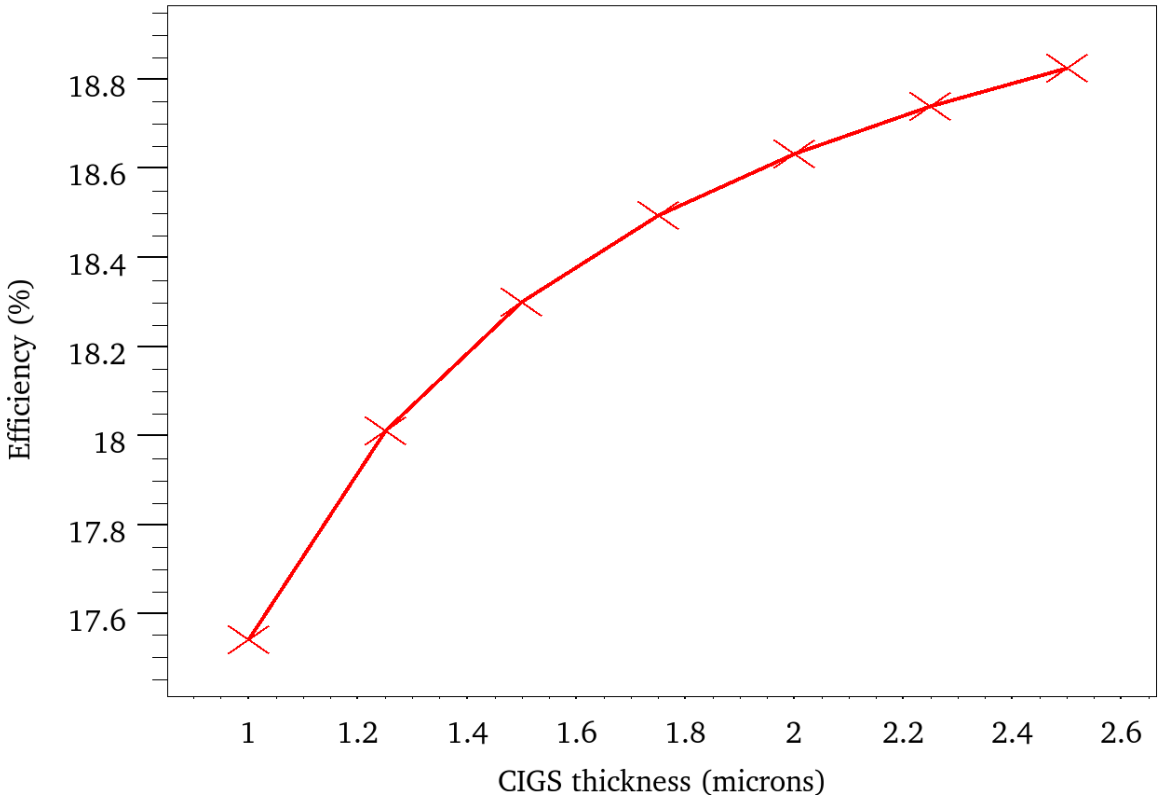

Figure 42. Sweep of CIGS thickness from 1.0 to 2.5 µm versus cell efficiency.

Table 7. Optimization trial run with corresponding thicknesses and efficiency.

Trial Run	CIGS(µm)	CdS(µm)	iZnO(µm)	Efficiency
1	2.25	0.05	0.05	18.763%
2	2.25	0.05	0.06	18.758%
3	2.25	0.06	0.05	18.800%
4	2.25	0.06	0.06	18.784%
5	2.50	0.05	0.05	18.849%
6	2.50	0.05	0.06	18.844%
7	2.50	0.06	0.05	18.886%
8	2.50	0.06	0.06	18.870%

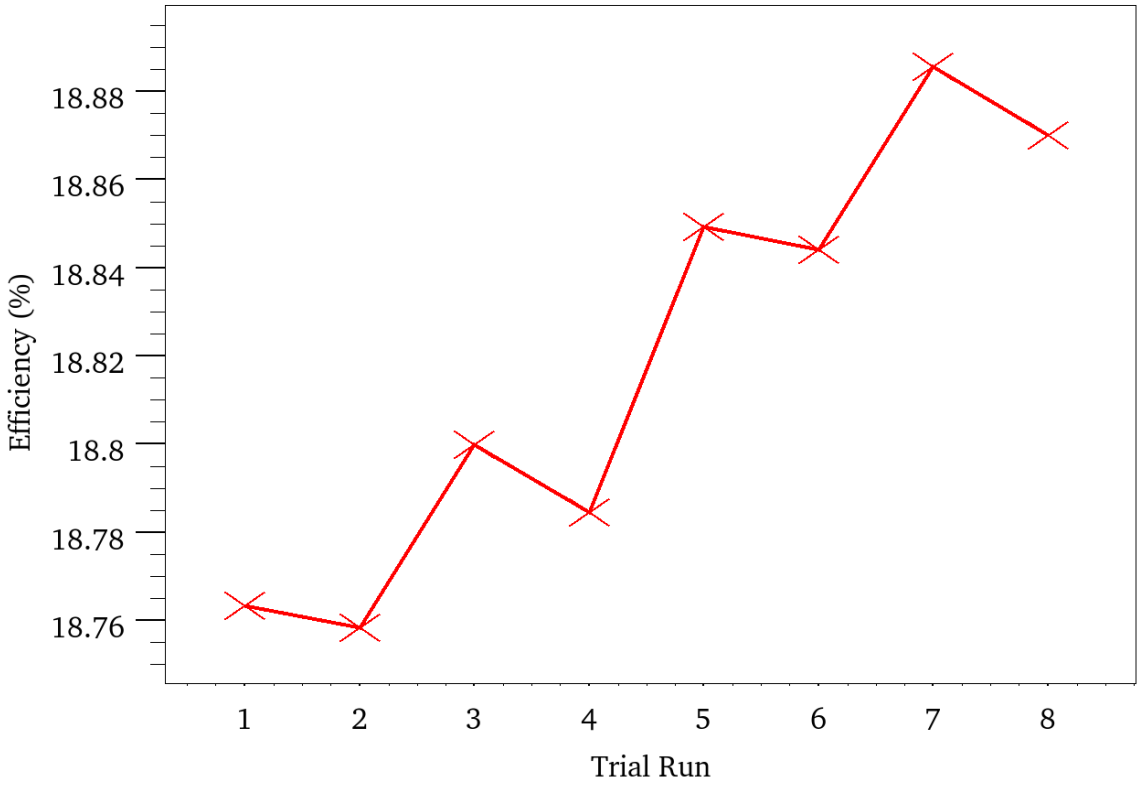

Figure 43. Optimization trial run from Table 7 versus cell efficiency.

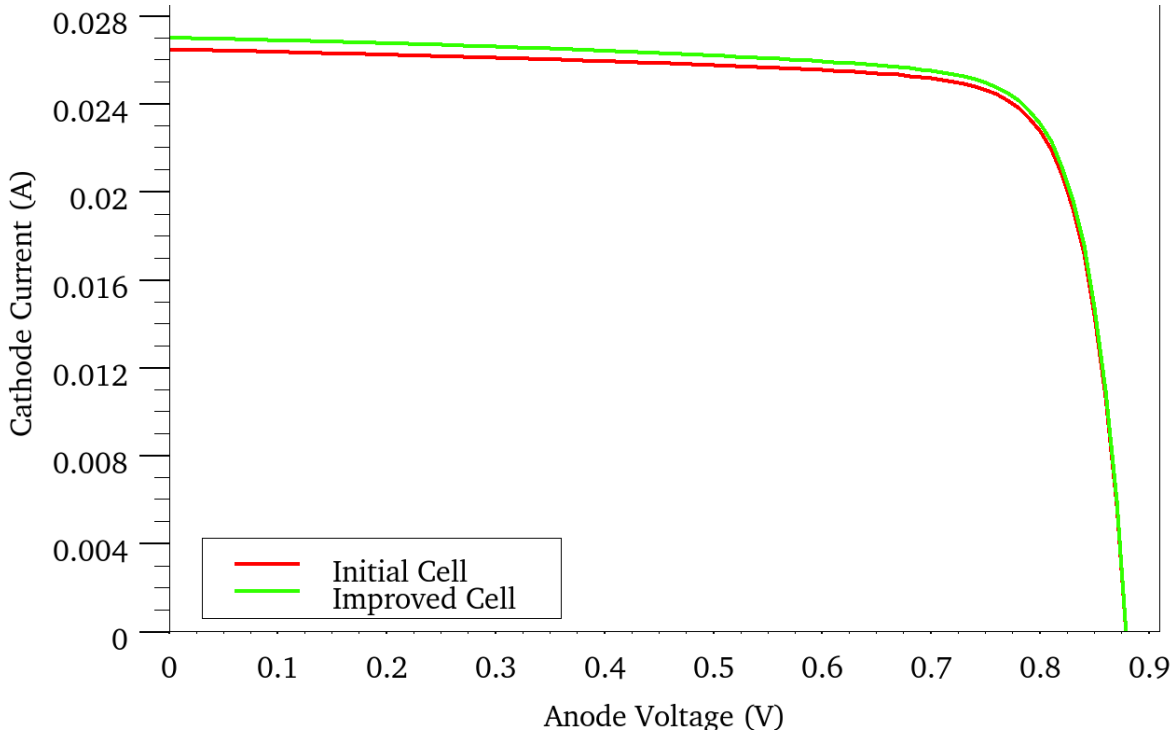

Figure 44. IV curves of initial cell and optimized cell.

C. GALLIUM OF 70% WITH BAND GAP OF 1.55 eV

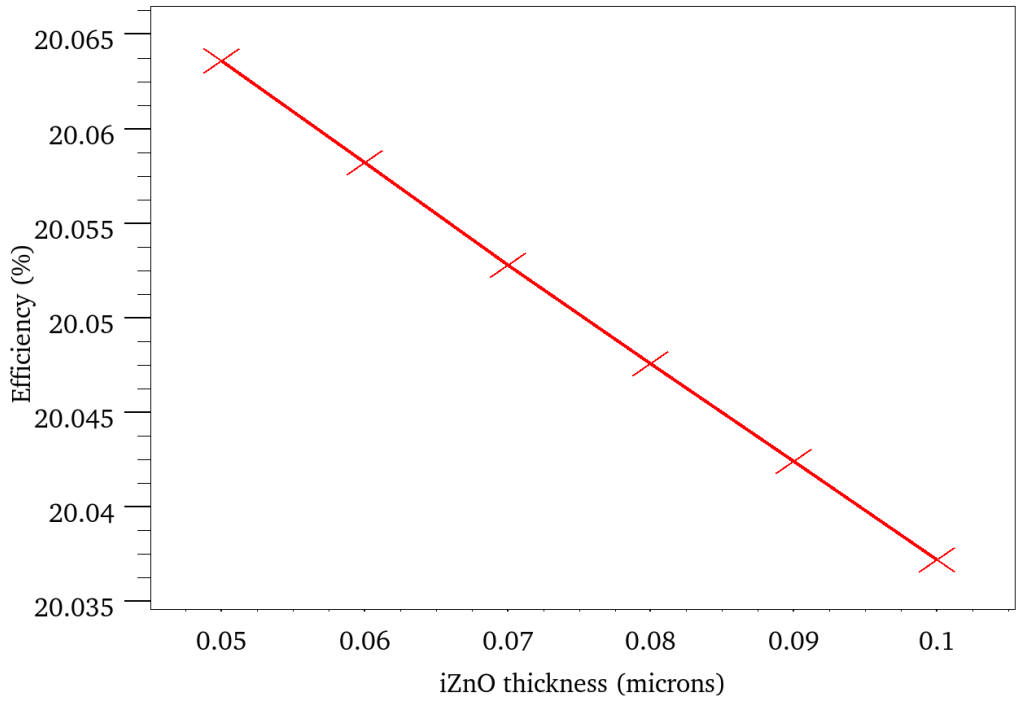

Figure 45. Sweep of iZnO thickness from 0.05 to 0.1 µm versus cell efficiency.

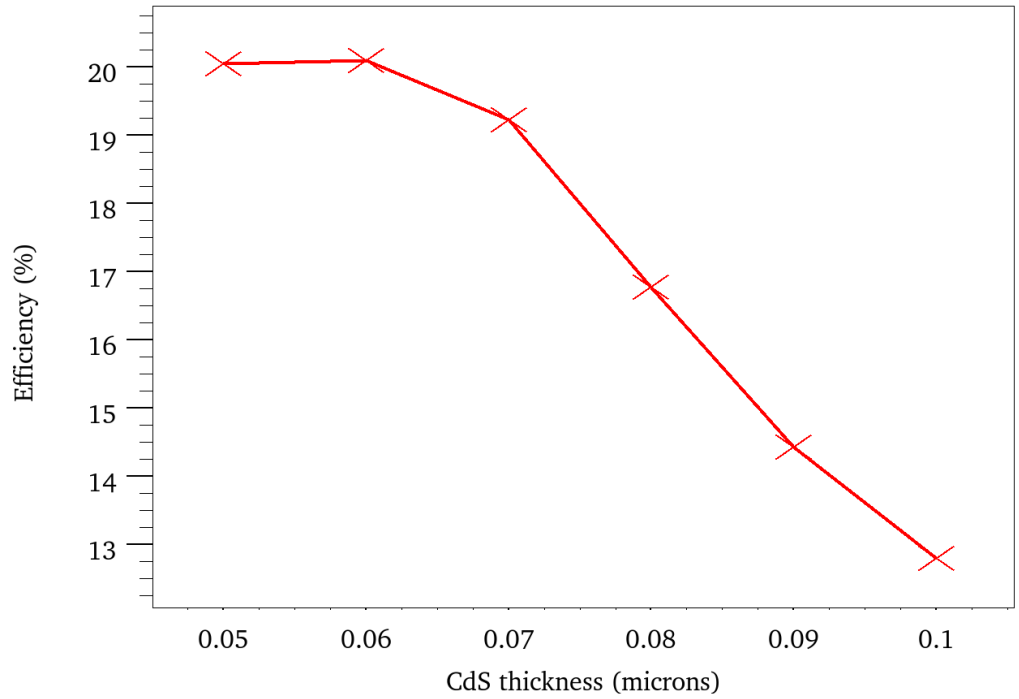

Figure 46. Sweep of CdS thickness from 0.05 to 0.1 µm versus cell efficiency.

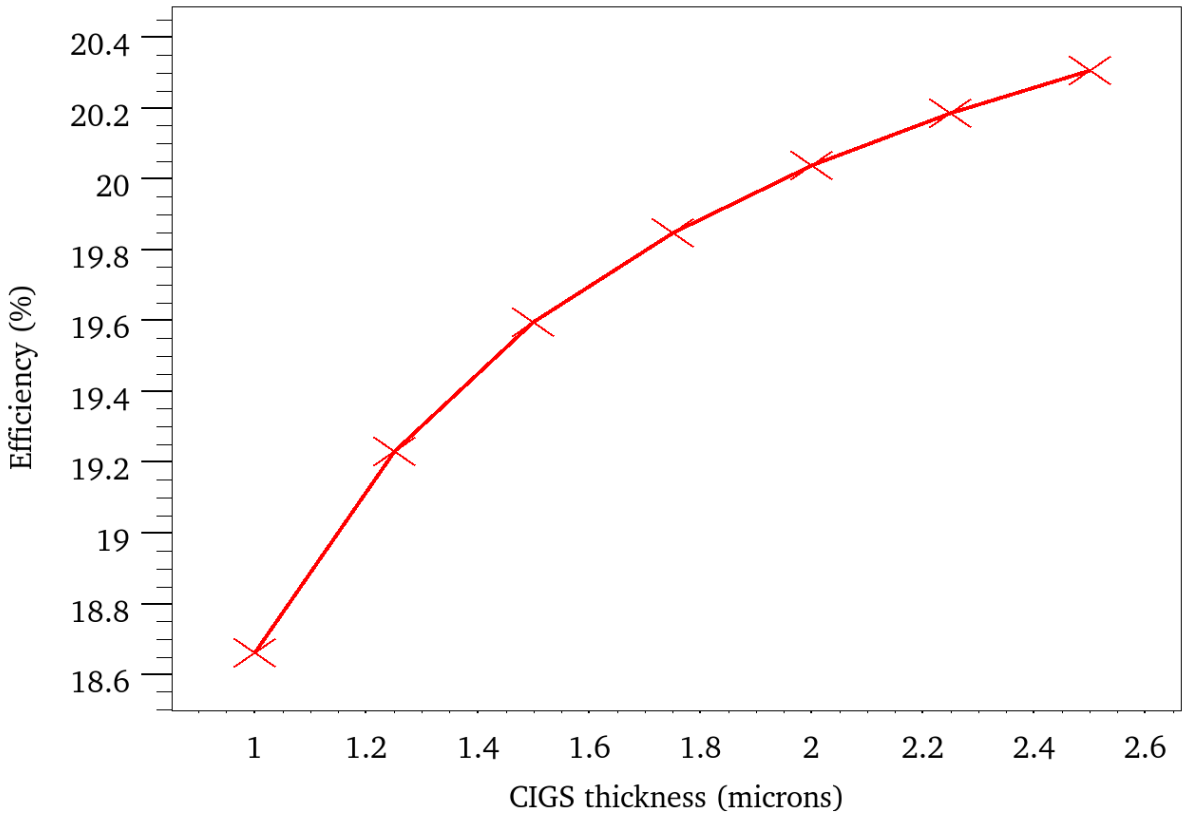

Figure 47. Sweep of CIGS thickness from 1.0 to 2.5 µm versus cell efficiency.

Table 8. Optimization trial run with corresponding thicknesses and efficiency.

Trial Run	CIGS(µm)	CdS(µm)	iZnO(µm)	Efficiency
1	2.25	0.05	0.05	20.212%
2	2.25	0.05	0.06	20.206%
3	2.25	0.06	0.05	20.277%
4	2.25	0.06	0.06	20.259%
5	2.50	0.05	0.05	20.334%
6	2.50	0.05	0.06	20.328%
7	2.50	0.06	0.05	20.398%
8	2.50	0.06	0.06	20.381%

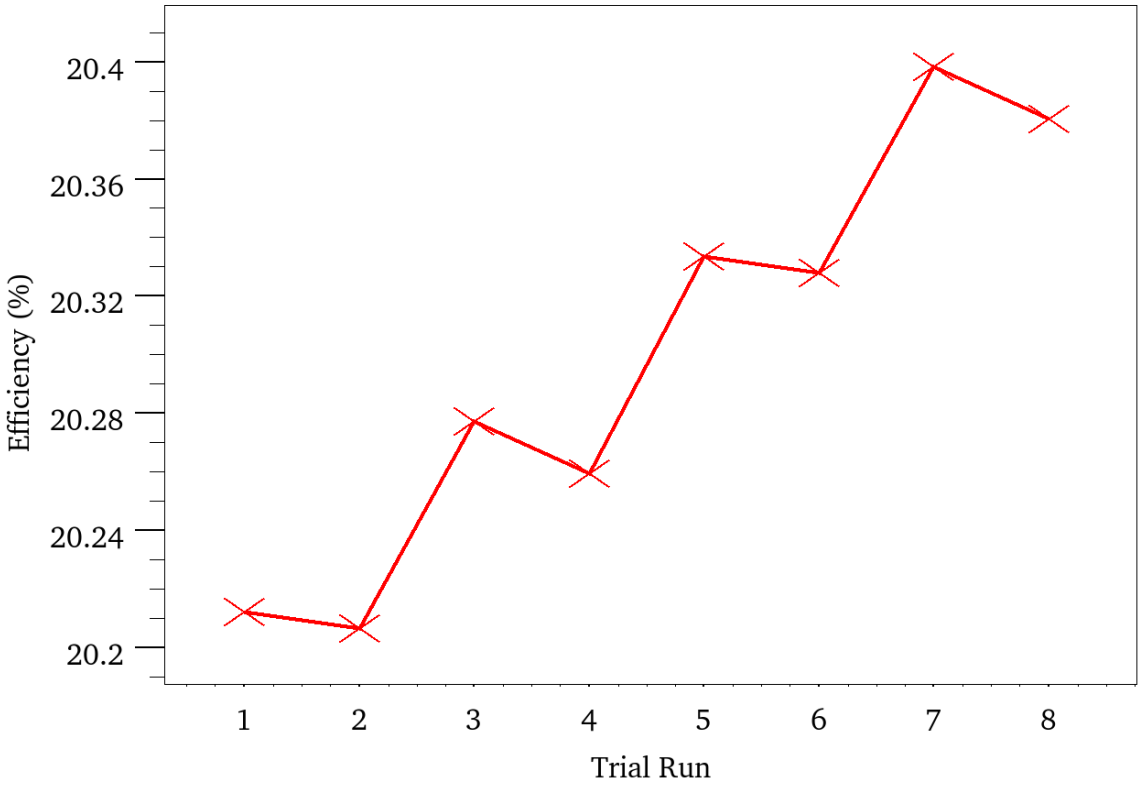

Figure 48. Optimization trial run from Table 8 versus cell efficiency.

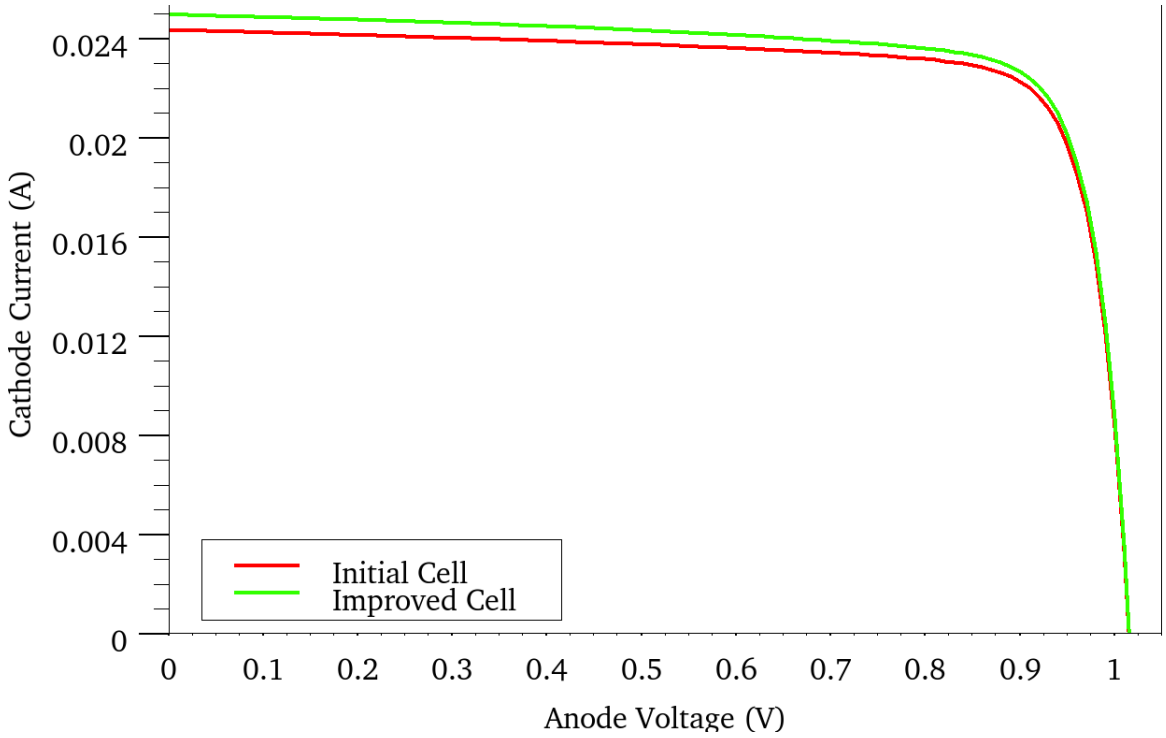

Figure 49. IV curves of initial cell and optimized cell.

D. GALLIUM OF 90% WITH BAND GAP OF 1.69 eV

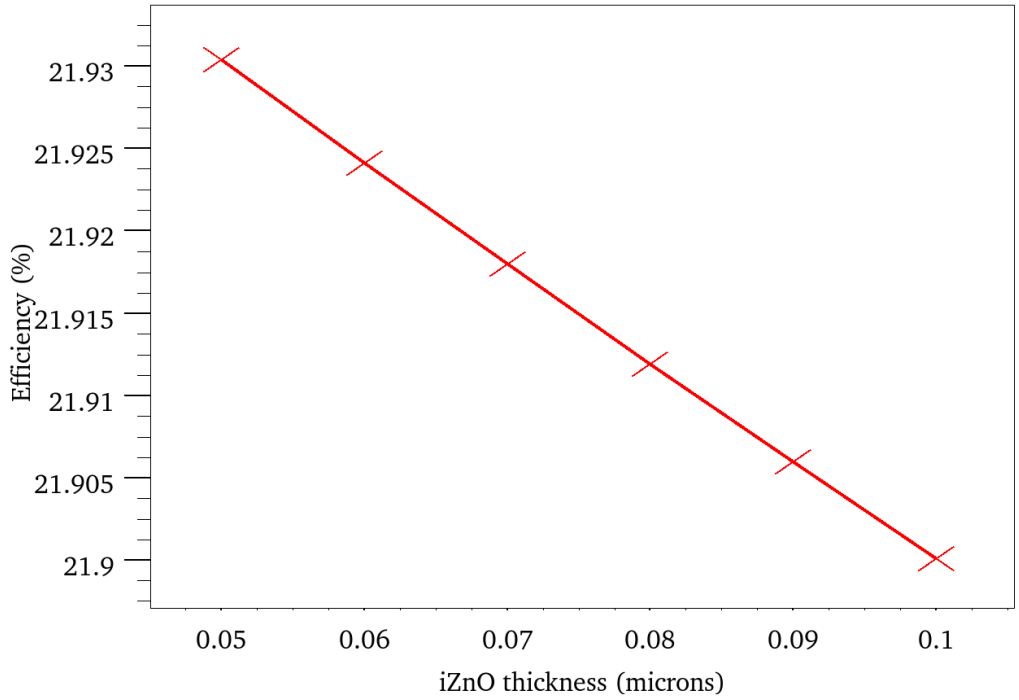

Figure 50. Sweep of iZnO thickness from 0.05 to 0.1 µm versus cell efficiency.

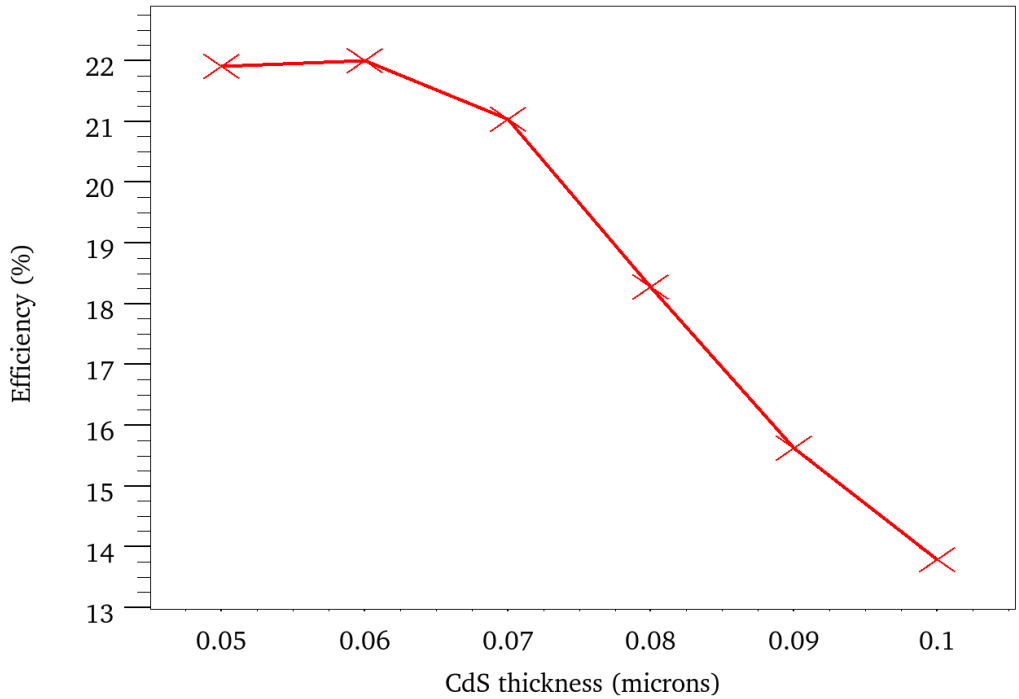

Figure 51. Sweep of CdS thickness from 0.05 to 0.1 µm versus cell efficiency.

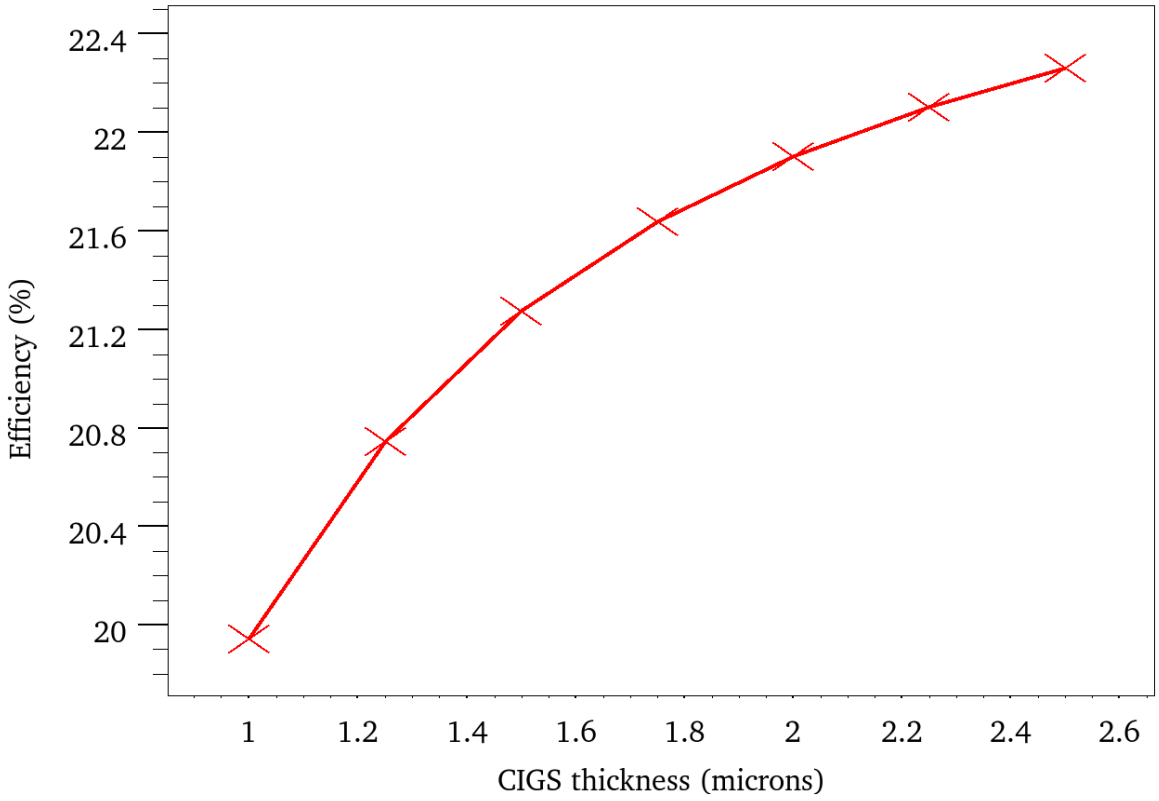

Figure 52. Sweep of CIGS thickness from 1.0 to 2.5 µm versus cell efficiency.

Table 9. Optimization trial run with corresponding thicknesses and efficiency.

Trial Run	CIGS(µm)	CdS(µm)	iZnO(µm)	Efficiency
1	2.25	0.05	0.05	22.132%
2	2.25	0.05	0.06	22.126%
3	2.25	0.06	0.05	22.244%
4	2.25	0.06	0.06	22.224%
5	2.50	0.05	0.05	22.292%
6	2.50	0.05	0.06	22.286%
7	2.50	0.06	0.05	22.404%
8	2.50	0.06	0.06	22.384%

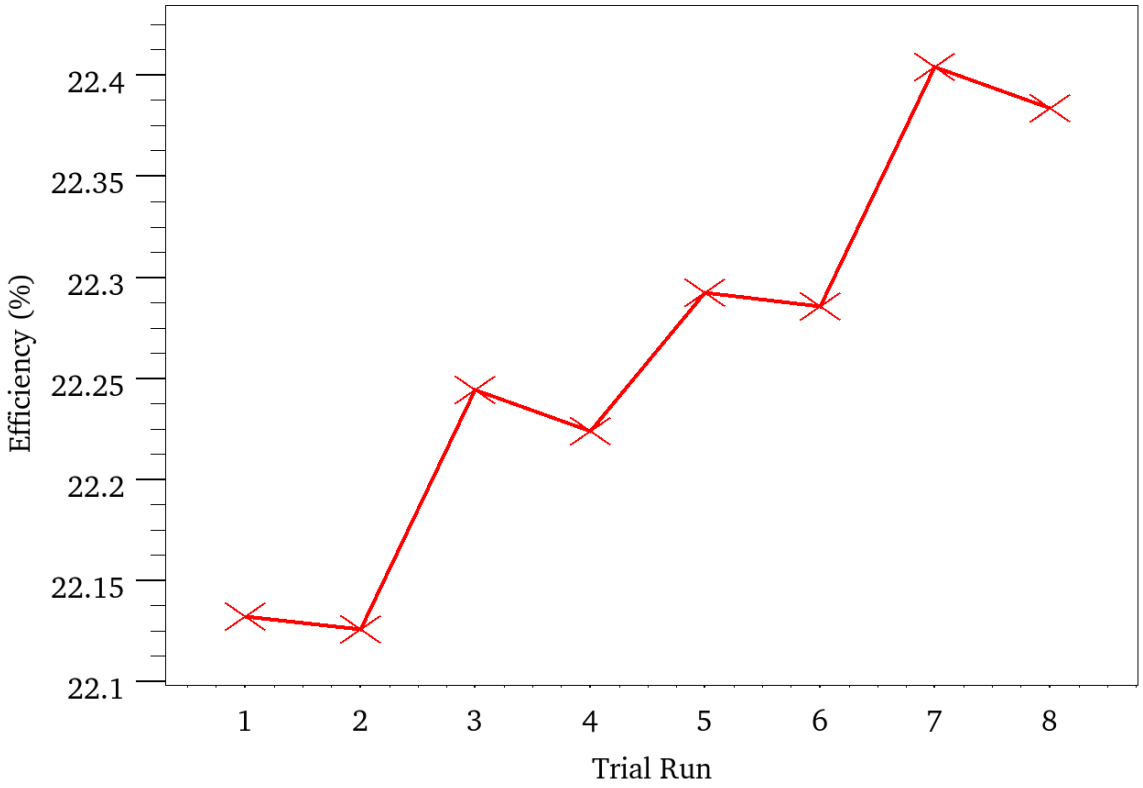

Figure 53. Optimization trial run from Table 9 versus cell efficiency.

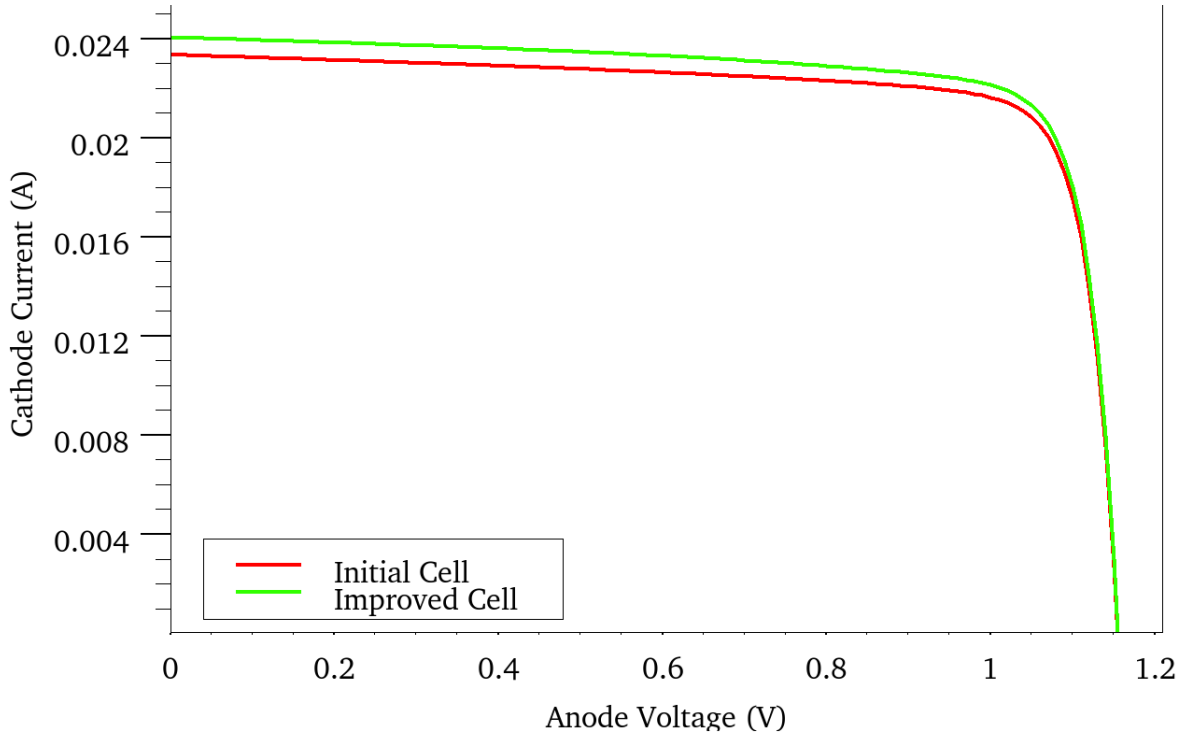

Figure 54. IV curves of initial cell and optimized cell.

LIST OF REFERENCES

[1] K. Fotis, "Modeling and simulation of a dual-junction CIGS solar cell using Silvaco ATLAS," M.S. thesis, Dept. Elec. Eng., Naval Postgraduate School, Monterey, CA, 2012.

[2] M. Hsieh, S. Kuo, F. Lai, M. Kao, P. Huang, H. W. Wang, M. Tsai, and H. Kuo, "Optimization of CdS buffer layer on the performance of copper indium gallium selenide solar cells," in *Proceedings of the International Quantum Electronics Conf. and Conf. on Lasers and Electro-Optics Pacific Rim,* Sydney, Australia, 2011, pp. 1532–1534.

[3] A. H. Jahagirdar, A. A. Kadam, N. and G. Dhere, "Role of i-ZnO in optimizing open circuit voltage of CIGS2 and CIGS thin film solar cells," in *Conf. Record of the IEEE 4th World Conf., Photovoltaic Energy Conversion,* Waikoloa, HI, 2006, pp. 557–559.

[4] T. Nakada, T. Kuraishi, T. Inoue, and T. Mise, "CIGS thin film solar cells on polymide foils," in *Photovoltaic Specialists Conf.*, Honolulu, HI, 2010, pp. 330-334.

[5] "United States Marine Corps expeditionary energy strategy and implementation plan," Headquarters, U.S. Marine Corps, Marine Corps Exped, Washington, DC, Feb. 2011.[Online]. Available: http://www.dtic.mil/dtic/tr/fulltext/u2/a541407.pdf

[6] Office of Naval Research. Ground Renewable Expeditionary Energy System [Online]. Available: http://www.onr.navy.mil/Media-Center/Fact-Sheets/Greens-Solar-Energy-Battery.aspx

[7] C. Hedelt. (Dec. 20, 2012). "MCSC helps Marines go green," Marine Corps Systems Command Corporate Communications. [Online]. Available: http://www.marcorsyscom.marines.mil/News/tabid/5830/Article/136008/mcsc-helps-marines-go-green.aspx

[8] A. R. Harvey, "The modification of HOMER software application to provide the United States Marine Corps with an energy planning tool," M.S. thesis, Dept. Elec. Eng., Naval Postgraduate School, Monterey, CA, 2012.

[9] D. Quick. (Nov. 8, 2013). Michele Combs a conservative voice for energy reform, *The Post and Courier* [Online]. Available: http://www.postandcourier.com/article/20131108/PC1208/131109503

[10] Triple-Junction ELO Tabbed Solar Cell for Portable Power Applications, MicroLink Devices, Inc., Niles, IL, 2012.

[11] U.S. Naval Research Laboratory, "High efficiency PV for expeditionary power," unpublished.

[12] A. Ripley, private communication, Apr. 2014.

[13] V. K. Kapur, V. K. Kapur, A. Bansal, and S. Roth, "Roadmap for manufacturing cost competitive CIGS modules," in *Photovoltaic Specialists Conference*, Austin, TX, 2012, pp. 3343–3348.

[14] Tactical Shelter Systems, ETI Tactical Shelters, [Online]. Available: http://www.isoshelters.com/

[15] S. Michael, "Renewable energy at military bases and for the warfighter," class notes for EC3240, Department of Electrical and Computer Engineering, Naval Postgraduate School, July, 2013.

[16] PV Education.Org, PN Junction [Online]. Available: http://pveducation.org/pvcdrom/pn-junction/doping

[17] A. S. Grove, "Elements of semiconductor" in *Physics and Technology of Semiconductor Devices*, New York: John Wiley and Sons, 1967, c. 4, pp. 91–106.

[18] *Wikipedia*, s.v. "p-n junction." [Online]. Available http://en.wikipedia.org/wiki/File:Pn-junction-equilibrium.png

[19] S.M. Sze, "Photodetectors and solar cells," *in Physics of Semiconductor Devices, 3rd ed*. Hoboken, NJ: Wiley-Interscience, 2007, ch. 13, pp. 663–742.

[20] L. C. Hirst and N. J. Ekins-Daukes, "Fundamental losses in solar cells," Dept. of Physics, Imperial College London, London, UK [Online]. Available https://workspace.imperial.ac.uk/quantumphotovoltaics/public/Hirst-EUPVSEC24.pdf

[21] *Encyclopedia of Alternate Energy*, s.v."Silicon" [Online]. Available: http://www.daviddarling.info/encyclopedia/S/AE_silicon.html

[22] B. Yan, G. Yue, J. Yang, and S. Guha, "High efficiency amorphous and nano-crystalline silicon thin film solar cells on flexible substrates," in *19th International Workshop, Active-Matrix Flatpanel Displays and Devices*, Kyoto, Japan, 2012, pp. 67–70.

[23] R. Yang, Z. Bai, D. Wang, and D. Wang, "High efficient thin film CdTe solar cells," in *Spanish Conference on Electron Devices*, Valladolid, Spain, 2013, pp. 341–344.

[24] *Wikipedia*, s.v. "Cadmium telluride thin film solar cell" [Online]. Available: http://en.wikipedia.org/wiki/File:Cadmium_telluride_thin_film_solar_cell.png

[25] A. Kanevce, "Anticipated performance of Cu(In,Ga)Se2 solar cells in the thin-film limit," Ph.D. dissertation, Dept. Physics, Colorado State Univ., Fort Collins, CO, 2007.

[26] V. Mohanakrishnaswarny, H. Sankaranarayanan, S. Pethe, C. S. Ferekides, and D. L. Morel, "The effect of Mo deposition condition on defect formation and device performance for CIGS solar cells," in *Photovoltaic Specialists Conference*, 2005, pp. 422-425.

[27] P. Reinhard, A. Chirila, P. Blosch, F. Pianezzi, S. Nishiwaki, S. Buecheler, and A. N. Tiwari, "Review of progress toward 20% efficiency flexible CIGS solar cells and manufacturing issues of solar modules" in *IEEE J. Photovoltaics,* vol. 3, no. 1, pp. 572-580, 2013.

[28] Atlas User's Manual, Silvaco Inc., Santa Clara, CA, 2013.

[29] W. N. Shafarman and L. Stolt, "Cu(InGa)Se2 solar cells," in *Handbook of Photovoltaic Science and Engineering,* Hoboken,: Wiley, 2003, ch. 13, pp. 567-616.

[30] R. Noufi and K. Zweibel, "High efficiency CdTe and CIGS thin-film solar cells: highlights and challenges" in *Conf. Record of the IEEE 4th World Conf., Photovoltaic Energy Conversion,* Waikoloa, HI, 2006, pp. 317-320.

[31] Solar World, Solar Energy 101, Making Solar Panels [online]. Available http://www.solarworld-usa.com/solar-101/making-solar-panels

[32] H. Sankaranarayanan, "Fabrication of CIGS absorber layers using a two-step process for thin film solar cell applications," Ph.D. dissertation, Dept. Elect. Eng., Univ. South Florida, Tampa, FL, 2004.

[33] Optics.Org. (2010 Nov. 01). Taiwan investors push Solarion to mass production [online]. Available http://optics.org/news/1/6/2

[34] J. V. Coba, "Application of Copper Indium Gallium Diselenide photovoltaic cells to extend the endurance and capabilities of the Raven RQ-11b unmanned aerial vehicle," M.S. thesis, Dept. Elec. Eng., NPS, Monterey, CA, 2010.

[35] National Renewable Energy Laboratory. National Center for Photovoltaics [online]. Available: http://www.nrel.gov/ncpv/

[36] F. Troni, F. Dodi, G. Sozzi, and R. Menozzi, "Modeling of thin-film Cu(In,Ga)Se_2 solar cells," in *Simulation of Semiconductor Processes and Devices* , Bologna, Italy, 2010, pp. 33-36.

THIS PAGE INTENTIONALLY LEFT BLANK

INITIAL DISTRIBUTION LIST

1. Defense Technical Information Center
   Ft. Belvoir, Virginia

2. Dudley Knox Library
   Naval Postgraduate School
   Monterey, California